PERGAMON Progress in Quantum Electronics 26 (2002) 65–130

Progress in Quantum Electronics

www.elsevier.com/locate/pquantelec

Review

Parametric characterization of the spatial structure of non-uniformly polarized laser beams

P.M. Mejías*, R. Martínez-Herrero, G. Piquero, J.M. Movilla

Departamento de Óptica, Facultad de Ciencias Físicas, Universidad Complutense de Madrid, 28040 Madrid, Spain

Abstract

We present an approach for describing the spatial structure of partially polarized light fields. Unlike the treatments usually encountered in the literature, in which the polarization state is represented by position-dependent functions, the formalism shown here characterizes the polarization by means of a family of measurable overall parameters averaged over the transverse spatial region where the beam intensity reaches significant values. Generalized degrees of polarization are introduced to evaluate the uniformity of the spatial distribution of the polarization state of the beam-like field. The possibility of improvement and optimization of the quality of a polarized laser beam (understood as the general usefulness of such field for collimation and focussing) is analyzed by employing first-order optical systems. Finally, attention is briefly devoted to non-paraxial electromagnetic vector beams, whose parametric description of their polarization properties constitutes, at present, a challenge for theoreticians.

PACS: 42.25.Ja; 42.55.−f; 42.60.Jf

Contents

*Corresponding author.
E-mail address: fiopt13@sis.ucm.es (P.M. Mejías).

0079-6727/02/$ - see front matter
PII: S0079-6727(02)00003-4

1. Introduction

Polarization refers to the vectorial nature of light fields. Due to the richness and significance of the properties that involve such vectorial behavior, the study of polarization-related phenomena has kept the attention of numerous scientists. The importance of this subject concerns theoretical topics in classical and quantum optics [1–5] as well as an extensive number of technological applications, which include biological optics, optical communications, atmospheric propagation, sensor devices and display technologies (see, for example Refs. [6–15]). But prior to handle the polarization properties, both an analytical description of the polarization state of the light disturbance and an associated measurement procedure should be established. As a matter of fact, the characterization process can be relevant in a number of related subjects. For instance:

(i) System design to measure and control the polarization. This is of use, for example, in the synthesis of polarized light and in optical metrology.
(ii) Sample-measuring polarimeters (the term sample includes optical elements, surfaces, thin films, biological materials, sensors, etc). These devices are used to

determine, for a given sample, the relationship between the polarization states of the incident and exiting beams.

(iii) Analysis of light sources and the involved emission processes. Laser sources are of special interest, including laser dynamics inside the cavity and other related phenomena.

As is well known, when one tries to characterize the polarization of a field, the simplest case corresponds to strictly-monochromatic (harmonic) plane waves: The end point of the electric vector then moves describing an ellipse, which may reduce in certain cases to a circle or a straight line. When the field, without being a plane wave, is well collimated, and its polarization is constant throughout the transversal cross-section, the formalism based on the Stokes parameters is revealed to be appropriate. However, in more realistic and general situations, beams depart from this simple model [16–27]. On the one hand, although the wavefronts of the beam-like fields have small angular spread (typical angular widths of a laser beam are of the order of milliradians), their intensity profiles take significant values only in a small transversal region around a mean axis (propagation direction). This is the typical behavior of the beams generated by laser emitters. On the other hand, the polarization has an intrinsic local character. In the literature, however, it is frequently encountered for most optical systems that the transmitted wavefront is assumed to have uniform (constant) polarization state. But, apart from the inherent point-dependent instrumental or residual polarization [28] of the non-ideal systems, current optical technologies that uses diffractive optical elements, polarization gratings or liquid crystals, to name only three, could involve devices in which the anisotropic behavior can change across the input and exit pupils of the optical element (this is of potential interest, for example, in interferometry and in optical information processing). For such systems and beams the above uniformity assumption fails. Moreover, in general, the polarization of a light beam generated by a partially coherent source changes under free propagation [29–35].

In conclusion, realistic beams, such as those emitted by laser cavities, exhibit, in general, spatially non-uniform distributions of their polarization state, which, in turn are modified when the beams travel through optical systems. In addition, the quasi-monochromatic beam-like fields quoted before have to be considered, in a general case, as both partially coherent and partially polarized from an spatial point of view.

The present paper deals with the problem of characterizing this kind of general non-uniformly polarized beams. In particular we will discuss in the following sections the characterization of their spatial structure by means of certain parameters and figures of merit that

(i) are valid for arbitrary beams,
(ii) are defined analytically in a rigorous way,
(iii) can be measured,
(iv) propagate according to simple laws through first-order optical systems.

This paper is then arranged as follows. The next section surveys the well-known existing formalism used to describe partially polarized beams. Special attention is devoted to justify, in a simple way, the quasi-transversality approximation that we

apply in the remainder of the paper. In addition, it is summarized in this section the basic content of the ISO/DIS 12005 document, concerning an international standard to evaluate the state and the degree of polarization of the light beams. The analytical and experimental limitations of this proposal are also briefly discussed. Section 3 introduces a physically meaningful scalar parametric description of the spatial structure of light beams, which constitutes the starting point for the vectoral parametric characterization developed in detail in Section 4. This vector formalism will enable us to define a new degree of polarization whose properties and measurement are illustrated by means of several examples in Section 5. Complementary information to that inferred from the above degree of polarization is provided by two other parameters, which are also reviewed in the same section. Section 6 deals with a beam quality parameter, which has revealed to be a useful tool to specify simultaneously the focussing properties of the beam at the near and at the far field. This figure of merit is defined for partially polarized beams. Improvement and optimization of this parameter by employing first-order polarizing optical systems is analyzed in the same section. In Section 7, the so-called electromagnetic vector beams will be considered. This kind of beams are receiving increasing attention in the last few years [36–50]. Here their interest arises from the fact that the paraxial and quasi-transversality assumptions we have supposed throughout this paper are removed. Finally, in Section 8, the main conclusions of this work are summarized.

2. Common representations of the polarization

To study the polarization properties of light fields, a single-vector description is applied in the majority of the cases of interest. More specifically, due to the nature of the detection processes usually involved in the measurements, the electric vector of the electromagnetic disturbance is chosen to be the vectorial quantity that represents the polarization state. Throughout the present paper we will follow an identical choice.

Next, we will briefly review the main calculi that have been developed for analysing polarization, namely, those based on the Jones matrix, the Mueller matrix and, more recently, on the so-called beam coherence-polarization (BCP) matrix [51–53]. All these formalisms represent the polarization of the field by means of functions (vectors or matrices) that explicitly depend on the position of typical points of the beam cross-section. This is the key conceptual difference with respect to the treatment we will introduce in the following sections, in which the polarization will be described by means of overall parameters, averaged (in a sense) over the transverse spatial regions where the beam intensity is significant.

2.1. The Jones calculus

Let us consider a coherent monochromatic plane wave whose electric field vector $\mathbf{E}$ has the form

$$\mathbf{E} = \begin{pmatrix} E_s \\ E_p \end{pmatrix} = \begin{pmatrix} a_s \exp[\mathrm{i}(kz - \omega t + \delta_s)] \\ a_p \exp[\mathrm{i}(kz - \omega t + \delta_p)] \end{pmatrix}, \tag{2.1}$$

where the subcripts s and p refer to the Cartesian components orthogonal to the direction of propagation z (see Fig. 1), k is the wavenumber of the light field, ω the angular frequency and the coefficients $a_j, \delta_j,\ j = s,p$, denote the amplitudes and phases associated to the transverse components. The Jones vector that represents this field is then defined as

$$\mathbf{E} = \begin{pmatrix} a_s \exp(\mathrm{i}\delta_s) \\ a_p \exp(\mathrm{i}\delta_p) \end{pmatrix}. \tag{2.2}$$

Note that both the amplitude and the polarization state of this field are uniform across any transverse plane.

Within the framework of the Jones calculus, the polarization properties of linear non-scattering optical systems can be described by means of a 2×2 matrix, the Jones matrix, which relates the exit and the incident fields passing through the optical element. We have

$$\mathbf{E}_{\text{output}} = \hat{J}\,\mathbf{E}_{\text{input}} = \begin{pmatrix} J_{11} & J_{12} \\ J_{21} & J_{22} \end{pmatrix} \begin{pmatrix} E_s \\ E_p \end{pmatrix}_{\text{input}}, \tag{2.3}$$

where $J_{nm},\ m,n = 1,2$, are, in general, complex elements and the letters surmounted by a caret will denote, from now on, matrices. Propagation through cascaded optical systems is then analyzed from the product of the successive Jones matrices, that is,

$$\hat{J} = \hat{J}_M \hat{J}_{M-1} \ldots \hat{J}_2 \hat{J}_1. \tag{2.4}$$

To end this short sketch of the Jones theory let us recall that each Jones matrix has two eigenpolarizations (or eigenvectors) $\mathbf{E}_\alpha$ and $\mathbf{E}_\beta$, which are transmitted by the system in the same polarization state and obey the eigenvalue equations

$$\hat{J}\,\mathbf{E}_\alpha = \alpha \mathbf{E}_\alpha, \tag{2.5}$$

$$\hat{J}\,\mathbf{E}_\beta = \beta \mathbf{E}_\beta. \tag{2.6}$$

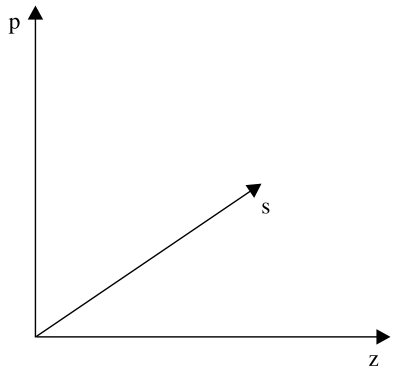

Fig. 1. Schematic of the Cartesian coordinate system. The plane wave propagates in the z-direction.

In addition, it can be shown that a Jones matrix can be written as a linear combination of the Pauli spin matrices [54,55]

$$\hat{J} = \sum_{m=0}^{3} c_m \hat{\sigma}_m, \tag{2.7}$$

where $\hat{\sigma}_0$ represents the 2×2 identity matrix

$$\hat{\sigma}_1 = \begin{pmatrix} 1 & 0 \\ 0 & -1 \end{pmatrix}, \qquad \hat{\sigma}_2 = \begin{pmatrix} 0 & 1 \\ 1 & 0 \end{pmatrix}, \qquad \hat{\sigma}_3 = \begin{pmatrix} 0 & -i \\ i & 0 \end{pmatrix} \tag{2.8}$$

and the coefficients c_m are complex numbers, which are closely related with the eigenvalues α and β by the formulae

$$\alpha = c_0 + (c_1^2 + c_2^2 + c_3^2)^{1/2}, \tag{2.9}$$

$$\beta = c_0 - (c_1^2 + c_2^2 + c_3^2)^{1/2}. \tag{2.10}$$

The Jones representation and the Pauli matrices will be handled in subsequent sections.

2.2. The quasi-transversality approach

The transversality condition for the electric field vector (i.e., **E** lies in planes orthogonal to the direction of propagation) assures us that the longitudinal component E_z vanishes. This provides a major simplification in the calculations. However, in practice, beam-like fields should be considered as a superposition of plane waves with slightly different directions, so that the beam spreads out under propagation. Moreover, it can be shown [36,37] that even the widely used linearly polarized Gaussian beam does not satisfy the Maxwell equations. These facts force us to take some care when we try to cancel the contribution of the vector component along the propagation direction, keeping only the transverse ones.

It can be proved [38,56] that, within the paraxial approximation, the longitudinal component of a beam-like field can be neglected to a good accuracy. Since this result is of major concern to characterize the polarization of a light field, we will next provide a simple demonstration of this approach.

For the sake of simplicity, only the coherent case will be explicitly considered. As before, the Cartesian electric vector components are denoted by $\mathbf{E} = (E_s, E_p, E_z)$, and we assume that the beam-like field is monochromatic and propagates through a non-magnetic, isotropic, homogeneous medium. Starting from the Maxwell equations, it is shown in many textbooks that the field components fulfill the Helmholtz equation:

$$\nabla^2 E_j + k^2 n^2 E_j = 0, \quad j = s, p, z, \tag{2.11}$$

where k is the wavenumber of the light and n represents the refractive index of the medium.

Let us now consider that the field exhibits a beam-like structure and remains essentially concentrated around the z-axis. If we assume long enough propagation distances z to neglect the contribution of evanescent waves, the electric vector

components, solution of the Helmholtz equations, can be expressed in terms of their angular plane-wave spectra in the form

$$E_j(x,y,z) = \int \tilde{E}_j(u,v)\exp\{\mathrm{i}kn[xu+yv+z(1-u^2-v^2)^{1/2}]\}\,\mathrm{d}u\,\mathrm{d}v,$$
$$j = s,p,z. \tag{2.12}$$

The function $\tilde{E}_j(u,v)$ can then be understood as the amplitude associated to a elementary plane-wave component traveling along the direction specified by the unit vector $(u,v,(1-u^2-v^2)^{1/2})$.

The paraxial regime is characterized by the condition [1,57,58]

$$u,v \ll 1, \tag{2.13}$$

which is consistent with the typical small angular width (also called divergence) of a laser beam. Consequently, the paraxial approximation follows from the substitution:

$$\exp\{\mathrm{i}knz[1-(u^2+v^2)]^{1/2}\} \simeq \exp(\mathrm{i}knz)\exp\left[-\mathrm{i}\frac{knz}{2}(u^2+v^2)\right] \tag{2.14}$$

in the exponential factor inside the integral of Eq. (2.12). We get

$$E_j(x,y,z) = \exp(\mathrm{i}knz)\int \tilde{E}_j(u,v)\exp[\mathrm{i}kn(xu+yv)]$$
$$\times \exp\left[-\mathrm{i}\frac{knz}{2}(u^2+v^2)\right]\mathrm{d}u\,\mathrm{d}v, \quad j = s,p,z. \tag{2.15}$$

We see that the vector components can formally be separated into a rapidly varying global phase factor in the longitudinal direction z and an amplitude that varies slowly in the s, p and z directions.

To proceed further, note that, for the media we are considering in this work, the electric field $\mathbf{E}$ obeys the Maxwell equation

$$\boldsymbol{\nabla}\cdot\mathbf{E} = 0, \tag{2.16}$$

which establishes a link between the respective plane-wave spectra $\tilde{E}_j(u,v)$, $j = s,p,z$, namely,

$$u\tilde{E}_s(u,v) + v\tilde{E}_p(u,v) + [1-(u^2+v^2)]^{1/2}\tilde{E}_z(u,v) = 0, \tag{2.17}$$

where again the evanescent wave are assumed to be negligible. Eq. (2.12) finally reads

$$\tilde{E}_z(u,v) = -\frac{u\tilde{E}_s(u,v) + v\tilde{E}_p(u,v)}{(1-u^2-v^2)^{1/2}}. \tag{2.18}$$

This expression allows us to evaluate the relative importance of the longitudinal electric field component with regard to the transverse ones: since in the paraxial regime $u,v \ll 1$ we have

$$\tilde{E}_z(u,v) \ll \tilde{E}_s(u,v), \tilde{E}_p(u,v). \tag{2.19}$$

In other words, we conclude that, within the framework of the paraxial limit, E_z can be neglected as compared with E_s and E_p. More precise analyses [38] show that the

longitudinal field amplitude is, in fact, two or three orders of magnitude smaller than the total field amplitude itself.

2.3. Polarization matrices

A complete description of the vectorial properties of a general electromagnetic field is provided by the tensorial theory of coherence developed by Wolf long ago [51,59,60]. The random light field, assumed to be stationary and ergodic (at least, up to second order) is determined by four coherence matrices, whose elements are

$$\mathscr{E}_{jk} = \langle E_j^*(\mathbf{r}_1, t) E_k(\mathbf{r}_2, t+\tau) \rangle_t, \tag{2.20}$$

$$\mathscr{H}_{jk} = \langle H_j^*(\mathbf{r}_1, t) H_k(\mathbf{r}_2, t+\tau) \rangle_t, \tag{2.21}$$

$$\mathscr{M}_{jk} = \langle E_j^*(\mathbf{r}_1, t) H_k(\mathbf{r}_2, t+\tau) \rangle_t, \tag{2.22}$$

$$\mathscr{N}_{jk} = \langle H_j^*(\mathbf{r}_1, t) E_k(\mathbf{r}_2, t+\tau) \rangle_t, \tag{2.23}$$

where E_j and H_k, $j,k = s,p,z$, represent again the three components of the electric and magnetic fields, respectively. In these equations $\mathbf{r}_1$ and $\mathbf{r}_2$ are position vectors, t is the temporal variable, τ a time interval and the symbol $\langle\ \rangle_t$ denotes a temporal average (since the field is ergodic, temporal and ensemble averages are equivalent). The elements of the coherence matrices are the correlations among the components of the electric and magnetic fields in two points, $\mathbf{r}_1$ and $\mathbf{r}_2$, evaluated at different times, t_1 and t_2, separated by the interval $t_2 - t_1 = \tau$. Note that the matrix elements do not depend on the time origin but only on the time difference τ because of the hypothesis of stationarity. In addition, since

$$\mathscr{M}_{kj}(\mathbf{r}_1, \mathbf{r}_2, \tau) = \mathscr{N}_{jk}^*(\mathbf{r}_2, \mathbf{r}_1, -\tau), \tag{2.24}$$

the matrices $\hat{\mathscr{M}}$ and $\hat{\mathscr{N}}$ are equivalent, and a set of 3×3 independent matrices would then suffice to characterize the electromagnetic field.

Let us now restrict ourselves to a single vector description and adopt the quasi-transversality approximation. In such a case, a single 2×2 matrix (the so-called covariance matrix $\hat{\Gamma}$) can be handled rather than the previous 3×3 coherence matrices. By choosing the z-axis as the effective direction of propagation of the beam-like field, the matrix $\hat{\Gamma}$ can be written in the form

$$\hat{\Gamma}(\mathbf{r}_1, \mathbf{r}_2, z; \tau) = \begin{pmatrix} \Gamma_{ss}(\mathbf{r}_1, \mathbf{r}_2, z; \tau) & \Gamma_{sp}(\mathbf{r}_1, \mathbf{r}_2, z; \tau) \\ \Gamma_{ps}(\mathbf{r}_1, \mathbf{r}_2, z; \tau) & \Gamma_{pp}(\mathbf{r}_1, \mathbf{r}_2, z; \tau) \end{pmatrix}, \tag{2.25}$$

where $\mathbf{r}_1$ and $\mathbf{r}_2$ are now position vectors lying in a plane $z =$ constant, and

$$\Gamma_{lm}(\mathbf{r}_1, \mathbf{r}_2, z; \tau) = \langle E_l^*(\mathbf{r}_1, z; t) E_m(\mathbf{r}_2, z; t+\tau) \rangle_t, \quad l,m = s,p. \tag{2.26}$$

Again s and p refer to Cartesian axes orthogonal to the direction of propagation z. Note that the covariance matrix is the natural vectorial generalization of the scalar mutual coherence function

$$\Gamma(\mathbf{r}_1, \mathbf{r}_2, \tau) = \langle E^*(\mathbf{r}_1, t) E(\mathbf{r}_2, t+\tau) \rangle_t. \tag{2.27}$$

In the present work we will focus our attention on quasi-monochromatic waves of mean frequency $\mathbf{v}$ and effective spectral width Δv. If we further suppose that any time delay introduced in the propagation process is small compared to the coherence time $1/\Delta v$, the covariance matrix becomes

$$\hat{\Gamma}(\mathbf{r}_1, \mathbf{r}_2, z) = \hat{G}(\mathbf{r}_1, \mathbf{r}_2, z) \exp(-2\pi i \mathbf{v}\tau), \tag{2.28}$$

where the matrix

$$\hat{G}(\mathbf{r}_1, \mathbf{r}_2, z) = \begin{pmatrix} G_{ss}(\mathbf{r}_1, \mathbf{r}_2, z) & G_{sp}(\mathbf{r}_1, \mathbf{r}_2, z) \\ G_{ps}(\mathbf{r}_1, \mathbf{r}_2, z) & G_{pp}(\mathbf{r}_1, \mathbf{r}_2, z) \end{pmatrix}, \tag{2.29}$$

is called beam coherence-polarization (BCP) matrix [52,53]. In the above equation the matrix elements $G_{lm}(\mathbf{r}_1, \mathbf{r}_2, z)$ denote the temporal averages $\langle E_l^*(\mathbf{r}_1, z; t) E_m(\mathbf{r}_2, z; t) \rangle_t$, where $l, m = s, p$. The BCP matrix provides a joint description of the polarization and spatial coherence properties of the beam. Its diagonal elements, G_{ss} and G_{pp}, could be regarded as the mutual intensities of the beam after crossing ideal linear polarizers whose transmission axes are the s-axis and the p-axis, respectively. Actually, $\hat{G}$ has only three independent elements, as follows from the relation between its non-diagonal elements:

$$G_{sp}(\mathbf{r}_1, \mathbf{r}_2, z) = G_{ps}^*(\mathbf{r}_2, \mathbf{r}_1, z). \tag{2.30}$$

Finally, it should be mentioned that all the elements of the BCP matrix could be considered measurable functions through certain Young interference experiments [53].

2.4. The Stokes–Mueller calculus

The local behavior of the polarization of a beam can be inferred from the BCP matrix with equal arguments $\mathbf{r}_1 = \mathbf{r}_2 = \mathbf{r}$, i.e., from the Hermitian matrix

$$\hat{G}(\mathbf{r}) = \begin{pmatrix} G_{ss}(\mathbf{r}) & G_{sp}(\mathbf{r}) \\ G_{ps}(\mathbf{r}) & G_{pp}(\mathbf{r}) \end{pmatrix}, \tag{2.31}$$

where

$$I(\mathbf{r}) = \mathrm{Tr}[\hat{G}(\mathbf{r})] = G_{ss}(\mathbf{r}) + G_{pp}(\mathbf{r}), \tag{2.32}$$

represents the intensity at each point $\mathbf{r}$ of the beam cross-section. In the above expression Tr stands for trace. To simplify the notation we omit the explicit dependence on z in the equations. An alternative four-parameter representation of polarized light is also provided by introducing the well-known Stokes vector $\mathbf{S}$, which is defined relative to a local coordinate in a plane perpendicular to the effective propagation axis of the beam. The components of this vector are the Stokes parameters, defined in terms of the elements of $\hat{G}$ as follows:

$$s_0(\mathbf{r}) = G_{ss}(\mathbf{r}) + G_{pp}(\mathbf{r}), \tag{2.33}$$

$$s_1(\mathbf{r}) = G_{ss}(\mathbf{r}) - G_{pp}(\mathbf{r}), \tag{2.34}$$

$$s_2(\mathbf{r}) = 2\,\mathrm{Re}[G_{sp}(\mathbf{r})], \tag{2.35}$$

$$s_3(\mathbf{r}) = 2\,\mathrm{Im}[G_{sp}(\mathbf{r})], \tag{2.36}$$

where Re[ ] and Im[ ] denote the real and imaginary parts, respectively. Since $G_{ss}G_{pp} - G_{sp}G_{ps} \geqslant 0$, we get the general condition

$$s_0^2(\mathbf{r}) \geqslant s_1^2(\mathbf{r}) + s_2^2(\mathbf{r}) + s_3^2(\mathbf{r}). \tag{2.37}$$

Furthermore, it is easy to see that the matrix $\hat{G}$ can be written in terms of these parameters in the form

$$\hat{G}(\mathbf{r}) = \tfrac{1}{2}[s_0(\mathbf{r})\hat{\sigma}_0 + s_1(\mathbf{r})\,\hat{\sigma}_1 + s_2(\mathbf{r})\hat{\sigma}_2 + s_3(\mathbf{r})\hat{\sigma}_3], \tag{2.38}$$

where $\hat{\sigma}_i$, $i = 0, 1, 2, 3$ are the Pauli matrices defined by Eq. (2.8) previously. This result closely resembles to that obtained for the Jones matrices. Taking this into account, the two eigenvalues, α_G and β_G, of the matrix $\hat{G}$ can be calculated from the Stokes parameters. We then have

$$\alpha_G = \tfrac{1}{2}[s_0 + (s_1^2 + s_2^2 + s_3^2)^{1/2}], \tag{2.39}$$

$$\beta_G = \tfrac{1}{2}[s_0 - (s_1^2 + s_2^2 + s_3^2)^{1/2}]. \tag{2.40}$$

The Stokes parameters are measurable quantities [15,54,61], which have also been employed, for example, in quantum mechanics [62]. In Optics, they are frequently used in connection with the Mueller calculus (see below) concerning the polarization description in irradiance-measuring devices, such as polarimeters and spectrometers, to mention only two. In addition, the Stokes parameters define the Poincare'sphere, that is, the unit sphere whose points, with coordinates (s_1, s_2, s_3), characterize the polarization state. Furthermore, within the framework of the density function approach [63,64] each state of partial polarization has been shown to be related to a probability distribution on the Poincaré sphere [65]. More specifically, the statistics of normalized and non-normalized Stokes parameters has been used to analyze light scattering by random media [65,66] as occurs, for example, in the characterization of random rough surfaces.

It would be desirable to describe the polarization state of a wave by means of a single parameter. This can be done by using the so-called degree of polarization, frequently encountered in the literature [54,61]. Since any quasi-monochromatic beam may be considered as a sum of a completely polarized and a completely unpolarized wave, independent each other, the degree of polarization is usually defined as the ratio of the intensity of the polarized part to the total intensity of the wave. It should be noted that, in general, such ratio will differ from one point to another. Hence we refer to it as the local degree of polarization $P(\mathbf{r})$, where $\mathbf{r}$ is, again, a position vector lying in a plane $z = \text{constant}$. This parameter has been expressed in equivalent forms, namely [52,54,61],

$$P(\mathbf{r}) = \left\{1 - \frac{4\,\det[\hat{G}(\mathbf{r})]}{\mathrm{Tr}[\hat{G}(\mathbf{r})]}\right\} = \frac{\alpha_G(\mathbf{r}) - \beta_G(\mathbf{r})}{\alpha_G(\mathbf{r}) + \beta_G(\mathbf{r})} = \frac{[s_1^2(\mathbf{r}) + s_2^2(\mathbf{r}) + s_3^2(\mathbf{r})]^{1/2}}{s_0^2(\mathbf{r})}, \tag{2.41}$$

where det denotes the determinant, and its value is independent of the choice of the transverse s- and p-axis, as expected. It is not difficult to show that $0 \leqslant P(\mathbf{r}) \leqslant 1$. The maximum value, $P(\mathbf{r}) = 1$, for every $\mathbf{r}$, correspond to uniformly totally polarized fields, and the minimum value, $P(\mathbf{r}) = 0$, for every $\mathbf{r}$, to unpolarized (natural) light.

Closely connected with the Stokes parameters we can define the Mueller matrix of an optical system as the 4×4 matrix $\hat{\mathscr{M}}$ which transform the Stokes vector of the incident beam into the Stokes vector of the exiting field, i.e. [28,67]

$$\mathbf{S}_{\text{out}} = \hat{\mathscr{M}}\mathbf{S}_{\text{in}} = \begin{pmatrix} m_{00} & m_{01} & m_{02} & m_{03} \\ m_{10} & m_{11} & m_{12} & m_{13} \\ m_{20} & m_{21} & m_{22} & m_{23} \\ m_{30} & m_{31} & m_{32} & m_{33} \end{pmatrix} \begin{pmatrix} s_0 \\ s_1 \\ s_2 \\ s_3 \end{pmatrix}_{\text{in}}, \tag{2.42}$$

where m_{ij}, $i,j = 0, 1, 2, 3$, are real valued elements, and the subscript in and out stand for the incident and exiting polarized fields, respectively. Moreover, the Mueller matrix associated to a sequence of cascaded polarizing instruments is given by the product of matrices of the individual optical elements.

In practice, Mueller matrices represent optical devices whose polarization-altering properties are uniform across the beam section. This makes the elements of the Mueller matrices of the common polarizing systems constant. Accordingly, the Mueller matrices form a subset of the 4×4 real matrices. Necessary conditions for physical realizability can be found, for example, in Refs. [28,68,69].

Let us finally recall that all Jones matrices have a corresponding Mueller matrix, although this is not a one-to-one mapping. For brevity, we omit here the correspondence relationships between both types of matrices $\hat{\mathscr{M}}$ and $\hat{J}$, which are given, for instance, in Ref. [68]. We will come back into the Stokes–Mueller formalism in Section 4.

2.5. ISO standards for polarization

We have seen in Section 2.3 that a quasi-monochromatic beam-like field is fully characterized (up to second order) by its BCP matrix. To determine its elements, conceptually simple measurement procedures can be proposed [53]. However, since the BCP matrix elements are complex-valued functions of five scalar space variables, the accurate implementation of such methods seems to be, in practice, a complicated and cumbersome task.

It would then be desirable to establish simple and fast-to-measure standards for characterizing the state and the degree of polarization of a light beam. This is the aim of the ISO 12005 document [70]. Let us then briefly describe the basis of this standard proposal.

The optical devices used to perform the measurements along with certain experimental requirements are listed below:

(i) *Power detector*: The output signal (voltage) should depend linearly on the input signal (laser power). A prior calibration procedure is needed.

(ii) *Linear polarizer*: The ratio T between its maximum and minimum transmission (associated with the two eigenpolarizations of the polarizer) should fulfill

$$T < \frac{1-p}{5p} \leqslant 0.02, \tag{2.43}$$

where p represents the degree of polarization of the beam to be measured. In other words, the use of a given polarizer is restricted by the polarization characteristics of the beam.

(iii) *Quarter-wave plate*: It should be designed to produce a phase difference between the two eigenpolarization of the element equal to $\lambda/4 \pm \lambda/200$, where λ is the mean wavelength of the beam.

(iv) *Optical attenuator*: It should be spatially uniform, without altering the polarization structure of the incident field.

The polarization of a beam is then evaluated from the determination of two contrast parameters, C_1 and C_2: First, we measure the maximum and minimum values of the beam power, $(W_1)_{\max}$ and $(W_1)_{\min}$, transmitted by a rotating linear polarizer (see Fig. 2a). One then gets

$$C_1 = \frac{(W_1)_{\max} - (W_1)_{\min}}{(W_1)_{\max} + (W_1)_{\min}}. \tag{2.44}$$

In a second step, a rotating quarter-wave plate is introduced between the source and the polarizer (see Fig. 2b). Both elements are rotated independently, and we measure again the maximum and minimum values, $(W_2)_{\max}$ and $(W_2)_{\min}$, of the transmitted power through the system. The parameter C_2 is defined in an analogous way to C_1:

$$C_2 = \frac{(W_2)_{\max} - (W_2)_{\min}}{(W_2)_{\max} + (W_2)_{\min}} \tag{2.45}$$

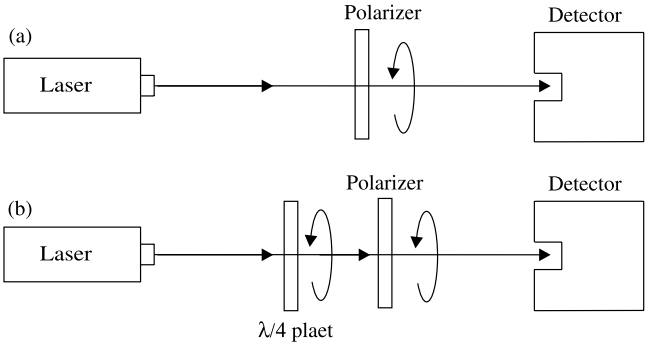

Fig. 2. (a) Schematic used to measure the parameter C_1. The polarizer is rotated around the central axis of the system. (b) Schematic used to measure the parameter C_2. Both the polarizer and the quarter-wave plate are now rotated.

with

$$0 \leqslant C_1, C_2 \leqslant 1. \tag{2.46}$$

The polarization state of the measured beam is then categorized following a similar procedure to that employed in the analysis of uniformly polarized planar waves. Thus, for example, if $C_1 > 0.9$, the beam is classified as totally polarized and its degree of polarization is considered to be equal to C_1. Furthermore, when $C_1, C_2 < 0.1$, the beam is said to be unpolarized. For brevity, we do not enter into more details of the ISO proposal, which the interested reader may find in Ref. [70].

It should be noted, however, that the experimental simplicity of the above classification standard method involves a price to pay, namely: (i) the lack of generality (the procedure essentially applies to uniformly polarized fields only), (ii) the absence of analytical propagation laws allowing to infer the polarization structure at some plane from the measured values at another previous plane, and (iii) the poor accuracy in the definitions used to classify the beams. Nevertheless, the ISO 12005 document should be considered a preliminary useful tool, valid for both continuous and pulsed beams (provided they are well stabilized in frequency and intensity), which deserves further attention in the future.

To end this section let us finally remark that use of the Stokes parameters, integrated throughout the beam cross-section, requires some caution: although the local values of these parameters $s_i(\mathbf{r})$, $i = 0, 1, 2, 3$, fully specify the polarization structure of any beam, however, a characterization based on the integrated Stokes parameters is only suited for uniformly polarized beams. For example, a radially symmetric linearly polarized beam whose intensity profile also exhibits radial symmetry would seem to be unpolarized from the values of the integrated Stokes parameters. Moreover, the same erroneous conclusion would be inferred from the application of the procedure proposed in the ISO 12005 document. This kind of discrimination problem will be discussed in Section 5.

3. Parametric characterization: scalar case

Before introducing a global characterization of polarized laser beams, it would be useful to provide a short survey of the key overall characteristic parameters that are commonly employed in the scalar framework. This will constitute the appropriate basis to treat, in subsequent sections, the vectorial behavior of the light beams. It should also be remarked that a number of these scalar overall parameters have been accepted as current ISO standards for laser beams.

3.1. Formalism and key parameters

A general (scalar) partially coherent field can be characterized (up to second order) by its cross-spectral density (CSD) function $W(\mathbf{r}_1, \mathbf{r}_2)$, defined in the form [1]

$$W(\mathbf{r}_1, \mathbf{r}_2, \omega) = \overline{\Psi^*(\mathbf{r}_1, \omega)\Psi(\mathbf{r}_2, \omega)}, \tag{3.1}$$

where Ψ denotes the field amplitude at frequency ω, $\mathbf{r}_1$ and $\mathbf{r}_2$ are two-dimensional position vectors transverse to the propagation direction z, and the overbar symbolizes an ensemble average. As is well known, the function W represents the correlation of the light field at two points $\mathbf{r}_1$ and $\mathbf{r}_2$ over the beam cross-section. Although, in terms of this function, the field propagation through optical systems can be analytically investigated in a rigorous way, however, the accurate experimental determination of the CSD constitutes a rather cumbersome task. This is particularly difficult for common multimode laser beams such as those emitted by Nd:YAG, excimer or high-power laser cavities.

It thus seems to be of more practical use to describe the spatial behavior of a light beam by means of global parameters or figures of merit that propagate according to simple laws. To do this let us first introduce the so-called Wigner distribution function (WDF), associated to the CSD through a Fourier transform relationship:

$$h(\mathbf{r}, \boldsymbol{\eta}, z) = \int_{-\infty}^{+\infty} W(\mathbf{r}, \mathbf{s}, z) \exp(\mathrm{i}k\boldsymbol{\eta} \cdot \mathbf{s})\, \mathrm{d}\mathbf{s}, \tag{3.2}$$

where $\mathbf{r} = (x, y)$ denotes the two-dimensional position vector orthogonal to the z-axis, $k\boldsymbol{\eta} = (ku, kv) = (k_x, k_y)$ gives the wavevector components along the Cartesian x- and y-axis, and $\mathbf{s}$ is a dummy vectorial variable. Again, u and v represent angles of propagation (without taking the evanescent waves into account). For simplicity, explicit dependence on temporal frequency ω has been omitted. Note that, in the above equation, the CSD function is defined in terms of the variables $\mathbf{r}$ and $\mathbf{s}$, which are related with $\mathbf{r}_1$ and $\mathbf{r}_2$ by the formulae

$$\mathbf{r} = \frac{\mathbf{r}_1 + \mathbf{r}_2}{2}, \qquad \mathbf{s} = \mathbf{r}_1 - \mathbf{r}_2. \tag{3.3}$$

In other words, $\mathbf{r}$ gives the middle point between $\mathbf{r}_1$ and $\mathbf{r}_2$ and $\mathbf{s}$ expresses their separation.

The WDF was defined by Wigner in quantum mechanics to describe the phenomena in the phase space (position-momentum) of the particles. Later Walther [71] introduced this function in Optics to link partial coherence with traditional radiometry. In a sense, the WDF can be physically understood in Optics as the amplitude associated to a ray passing through a point along a certain direction. It should be noted, however, that unlike the positiveness of the energy content of a ray, the WDF could take negative values in some cases [72,73]. Nevertheless, from the WDF it is possible to define a number of parameters closely related with radiometric concepts. As a matter of fact, integration of $h(\mathbf{r}, \boldsymbol{\eta}, z)$ over the angular variables u and v is proportional to the beam irradiance. Furthermore, integration over the spatial variables x and y gives the directional intensity, which is proportional to the radiant intensity of the field (a factor $\cos^2 \beta$ apart, where β is the angle of observation).

In addition, the so-called beam intensity moments can be rigorously defined as follows:

$$\langle x^m y^n u^p v^q \rangle \equiv \frac{1}{I_0} \int \int_{-\infty}^{+\infty} x^m y^n u^p v^q h(\mathbf{r}, \boldsymbol{\eta}, z)\, \mathrm{d}\mathbf{r}\, \mathrm{d}\boldsymbol{\eta}, \tag{3.4}$$

where m, n, p, q are integer numbers, the sharp brackets $\langle\ \rangle$ are defined by Eq. (3.4) itself, and

$$I_0 = \int\int_{-\infty}^{+\infty} h(\mathbf{r}, \boldsymbol{\eta}, z)\, \mathrm{d}\mathbf{r}\, \mathrm{d}\boldsymbol{\eta}, \tag{3.5}$$

is proportional to the total irradiance.

The four first-order beam moments, namely, $\langle x \rangle$, $\langle y \rangle$, $\langle u \rangle$ and $\langle v \rangle$, characterize the center of the beam and its mean direction. For the sake of simplicity, in what follows it will be assumed that these moments equal zero. This is not a true restriction, since it is equivalent to a shift of the Cartesian coordinate system.

The ten different second-order moments are shown to be closely related with the spatial structure of the beam. In terms of them, the following physically meaningful characteristic parameters have been introduced in the literature (see, for example Refs. [74–80]):

- The (squared) beam width at a plane $z =$ constant (i.e., the spatial size of the cross-section where the intensity takes significant values) is represented by $\langle x^2 + y^2 \rangle$, where $\langle x^2 \rangle$ and $\langle y^2 \rangle$ are the (squared) transverse beam widths along the x- and y-axis, respectively (see Fig. 3). In terms of the beam intensity, $I(x, y)$, we have

$$\langle x^2 + y^2 \rangle = \frac{\int\int_{-\infty}^{+\infty} (x^2 + y^2)\, I(x, y)\, \mathrm{d}x\, \mathrm{d}y}{\int\int_{-\infty}^{+\infty} I(x, y)\, \mathrm{d}x\, \mathrm{d}y}. \tag{3.6}$$

- $\langle u^2 + v^2 \rangle$ is a measure of the (squared) far-field divergence, which is connected with the energy distribution associated with each spatial frequency of the beam.
- $\langle xu + yv \rangle$ gives the position of the beam waist, i.e., the plane where the beam width takes its minimum value (see Fig. 3). More specifically, $\langle xu + yv \rangle$ vanishes at such plane. In addition, $\langle xu \rangle$ and $\langle yv \rangle$ are related to the curvature radii of the beam by the formulae

$$R_x = \frac{\langle x^2 \rangle}{\langle xu \rangle}, \qquad R_y = \frac{\langle y^2 \rangle}{\langle yv \rangle}. \tag{3.7}$$

- $\langle xy \rangle$ provides the orientation of the so-called principal axis of the beam through the condition $\langle xy \rangle = 0$ [81]. The beam widths $\langle x^2 \rangle^{1/2}$ and $\langle y^2 \rangle^{1/2}$ reach their extreme (maximum and minimum) values along the principal axes (see Fig. 4). Since, in general, the spatial profile rotates as the field propagates in free space, these axes can be used to determine the orientation of the beam profile.
- $\langle uv \rangle$ gives the orientation of the so-called absolute axes of the beam [81], which are defined by the condition $\langle uv \rangle = 0$. Unlike the principal axes, the absolute axes do not rotate upon free propagation, so that they constitute an absolute transverse coordinate system with respect to which the orientation of the principal axes is fixed.
- The difference $\langle xv \rangle - \langle yu \rangle$ is related with the orbital angular momentum of the beam. The angular momentum is responsible for the twisting spatial behavior

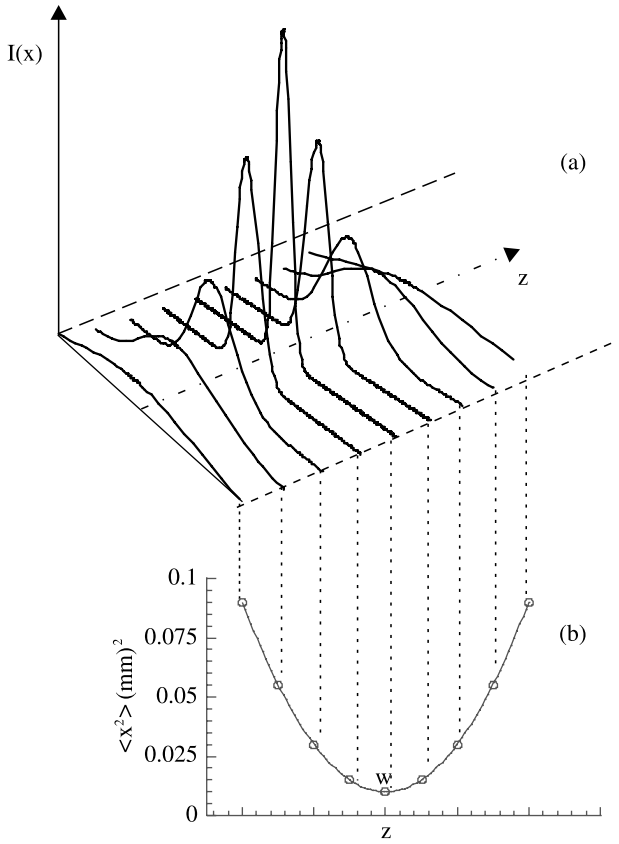

Fig. 3. Free propagation of a (one-dimensional) Gaussian beam ($\lambda = 633$ nm). (a) Transverse intensity profiles at different planes z =constant. (b) Parabolic dependence of the second-order moment $\langle x^2 \rangle$ on the propagation distance z. The value w designates the position of the waist (minimum beam width). The separation between the successive planes plotted in the figure is 125 mm.

displayed by some type of beams under propagation (see Fig. 5). In fact, the time averaged orbital angular momentum flux J_z transported by the beam through a plane z =constant is given by [82]

$$J_z = \frac{I_0}{c}(\langle xv \rangle - \langle yu \rangle), \tag{3.8}$$

where c is the speed of light. In particular, J_z vanishes for rotationally symmetric Gaussian beams as well as for Hermite–Gauss beams, but it differs from zero for twisted Gaussian beams or for certain rotationally symmetric Laguerre–Gauss beams.

- Finally, other useful parameter that can be expressed in terms of second-order moments, is the Rayleigh range, z_R, which represents the distance that a beam must propagate in free space to duplicate its (squared) width. This parameter can

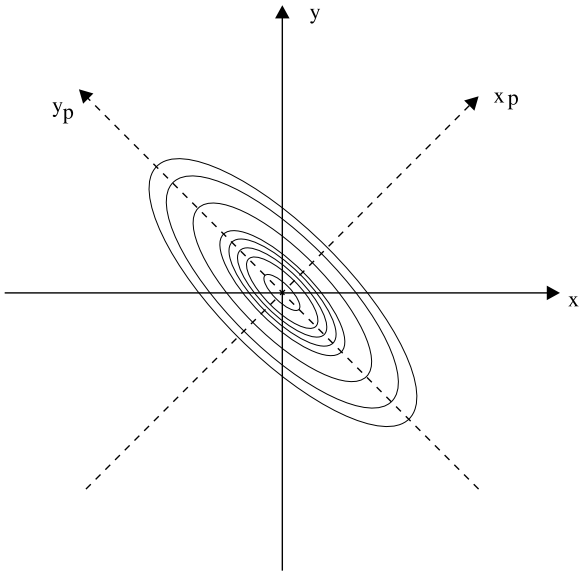

Fig. 4. Geometrical meaning of the second-order moment $\langle xy \rangle$. Isophotes (contour lines of equal intensity) of an astigmatic Gaussian beam profile at a plane transverse to the propagation direction z. The principal axes are denoted by x_p, y_p.

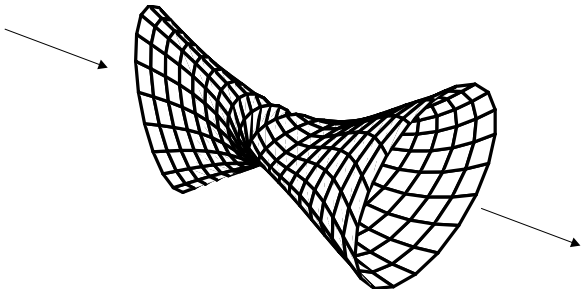

Fig. 5. Illustrating the spatial behavior under free propagation of a twisted Gaussian beam. The arrows indicate the propagation direction of the beam.

be defined as follows:

$$z_{\mathrm{R}} = \left(\frac{\langle r^2 \rangle_{\mathrm{w}}}{\langle \eta^2 \rangle} \right)^{1/2}, \tag{3.9}$$

where the subscript w indicates that the moment is evaluated at the waist plane.

Some higher-order moments of the WDF are also of interest. In particular, certain fourth-order moment, namely, the kurtosis, has been shown to quantify the sharpness of the beam [83–87]. Moreover, a number of combinations of the intensity moments give rise to invariant parameters [88–91]. Among them, the so-called beam

quality factor has demonstrated to be of special relevance [88,92–95]. For brevity, we refer the reader to Section 6.

To analytically handle in a compact way the second-order moments of a beam it is useful to arrange them in a 4×4 symmetric matrix, $\hat{M}$, defined at a certain plane in the form

$$\hat{M} = \begin{pmatrix} \langle x^2 \rangle & \langle xy \rangle & \langle xu \rangle & \langle xv \rangle \\ \langle xy \rangle & \langle y^2 \rangle & \langle yu \rangle & \langle yv \rangle \\ \langle xu \rangle & \langle yu \rangle & \langle u^2 \rangle & \langle uv \rangle \\ \langle xv \rangle & \langle yv \rangle & \langle uv \rangle & \langle v^2 \rangle \end{pmatrix}. \tag{3.10}$$

The importance of this matrix arises from the following major properties:

(i) All the elements of $\hat{M}$ are measurable quantities, and can be obtained from the beam intensity values at certain planes.

(ii) The value of $\hat{M}$ at the output plane of any first-order optical system can be inferred from the measured values of its elements at the input plane by application of the simple paraxial law [88]

$$\hat{M}_{\mathrm{o}} = \hat{\mathscr{S}} \hat{M}_{\mathrm{i}} \hat{\mathscr{S}}^{\mathrm{t}}, \tag{3.11}$$

where $\hat{\mathscr{S}}$ is the 4×4 ABCD matrix which represents the optical system, t denotes transposition and the subscript "o" and "i" refer to the output and input planes, respectively.

3.2. Measurement of the second-order intensity moments

To conclude this section let us say a few words about the measurement procedure of the above laser beam parameters. Experiments currently employ CCD cameras or similar devices such as pyroelectric matrix arrays [96]. Apart from the spatial resolution limit fixed by the pixel size of the camera, the main experimental limitation comes from the signal-to-noise ratio of the output signal. Light scattering, defective pixels, background noise and electronic circuitry, among other noise sources, would actually reduce the performance of the measurement optical devices. Consequently, a careful measurement process is, in general, required.

The basic method records the beam intensity profile $I(x, y, z)$ at different planes by means of a CCD (or pyroelectric) camera. From the data supplied by the camera (intensity versus position), a laser beam-analyzer software computes the purely spatial moments $\langle x^2 \rangle$, $\langle y^2 \rangle$ and $\langle xy \rangle$. It is easy to see that they propagate in free space according to a parabolic law, namely

$$\langle x^2 \rangle_{z_2} = \langle x^2 \rangle_{z_1} + 2\langle xu \rangle_{z_1}(z_2 - z_1) + \langle u^2 \rangle_{z_1}(z_2 - z_1)^2, \tag{3.12}$$

$$\langle y^2 \rangle_{z_2} = \langle y^2 \rangle_{z_1} + 2\langle yv \rangle_{z_1}(z_2 - z_1) + \langle v^2 \rangle_{z_1}(z_2 - z_1)^2, \tag{3.13}$$

$$\langle xy \rangle_{z_2} = \langle xy \rangle_{z_1} + (\langle xv \rangle_{z_1} + \langle yu \rangle_{z_1})(z_2 - z_1) + \langle uv \rangle_{z_1}(z_2 - z_1)^2. \tag{3.14}$$

In these equations the subscript z_2 indicates the plane where the spatial intensity moments are measured, and the subscript z_1 denotes the plane where the intensity moments should be determined.

By using a fitting procedure of the experimental data to the parabolic curves given by Eqs. (3.12)–(3.14), we could obtain eight second-order moments (see Fig. 6). It would remain, however, to get the moments $\langle xv\rangle_{z_1}$ and $\langle yu\rangle_{z_1}$, since they are coupled by Eq. (3.14). Consequently, additional measurements are needed [97,98]. The usual procedure then follows two steps:

Step 1: At plane $z = z_2$ we set a cylindrical lens L_1 whose axis makes an angle 45° with the x-axis. We then have (cf. Eq. (3.11))

$$\langle xv\rangle_{z_2} - \langle yu\rangle_{z_2} = f_{cyl}[\langle v^2\rangle_{z_3} + \langle v^2\rangle_{z_2} - \langle u^2\rangle_{z_2} - \langle u^2\rangle_{z_3}] + \langle xu\rangle_{z_2} - \langle yv\rangle_{z_2}, \tag{3.15}$$

where the subscript z_3 refers to the output plane of L_1, f_{cyl} denotes the focal length of the lens and $\langle xu\rangle_{z_2}$ and $\langle yv\rangle_{z_2}$ are experimental data.

Step 2: After L_1 we now place a second (spherical) lens L_2 (see Fig. 7) and measure the transverse beam widths over its paraxial focal plane $z = z_4$. We get

$$\langle u^2\rangle_{z_3} = \frac{\langle x^2\rangle_{z_4}}{f_{esf}^2}, \tag{3.16}$$

$$\langle v^2\rangle_{z_3} = \frac{\langle y^2\rangle_{z_4}}{f_{esf}^2}, \tag{3.17}$$

where f_{esf} represents the focal length of L_2, and $\langle x^2\rangle_{z_4}$ and $\langle y^2\rangle_{z_4}$ are experimental data. From the combination of Eqs. (3.14)–(3.17), the crossed moments $\langle xv\rangle_{z_1}$ and $\langle yu\rangle_{z_1}$ are finally inferred.

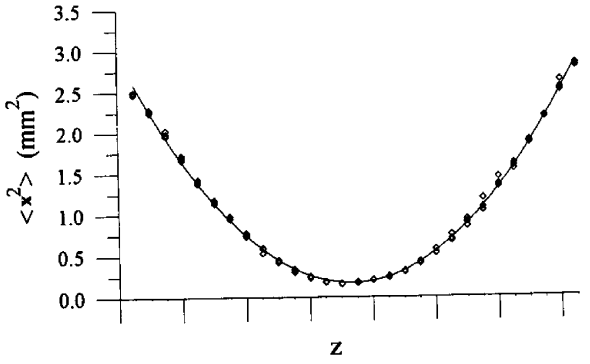

Fig. 6. Squared beam width $\langle x^2\rangle$ versus propagation distance z (in abscises, the distance between divisions is 200 mm). The rhombus represent the experimental values, which correspond to a beam emitted by a CO_2 laser [96]. The continuous line is the parabolic curve that best fits the data. At each plane z =constant three measurement of $\langle x^2\rangle$ were performed with a pyroelectric camera. The plane where the parabola reaches its minimum determines the waist plane of the beam.

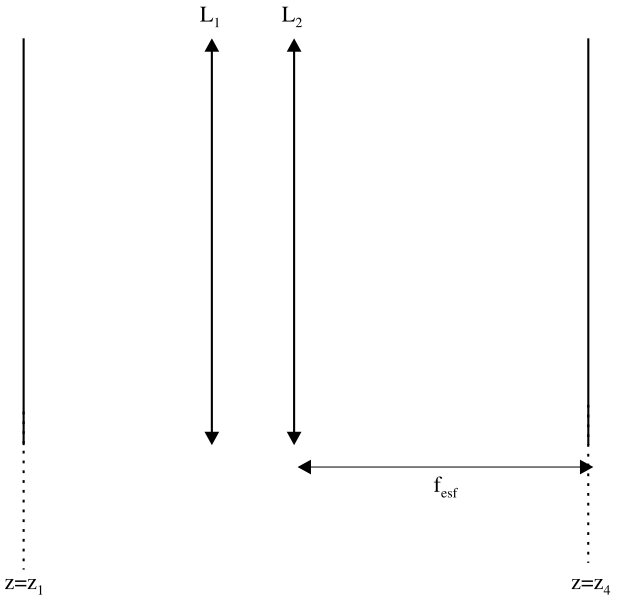

Fig. 7. Decoupling and measurement of the second-order moments $\langle xv \rangle$ and $\langle yu \rangle$. For clarity, lenses L_1 and L_2 are represented in separate planes in the figure. Note, however, that these lenses are put together in the experimental arrangement.

4. Parametric characterization: vectorial case

In Section 2 we recalled that partially polarized beams and polarization-altering optical systems could be handled by using four-component Stokes vectors and Mueller matrices, respectively. To apply such general formalism, most papers assume, however, a uniform polarization state across transverse planes. In the present section we generalize the Stokes representation in order to link the spatial structure of the light beam with its polarization features. This would also provide the mathematical tool to appropriately describe the evolution of the transverse profile of the beam as it propagates through optical systems. As we will see later, this formalism exhibits strong similarities with both the spatial scalar treatment summarized in the previous section and the usual Mueller framework.

4.1. The Wigner matrix

Let us again consider an electromagnetic field understood as an ergodic stationary random process propagating as a beam along the z-axis. Assuming the quasi-transversality condition within the paraxial approximation, the associated electric field vector at frequency ω, perpendicular to the z-axis may be written as

$$\mathbf{E}(\mathbf{r}, z; \omega) = (E_s(\mathbf{r}, z; \omega), E_p(\mathbf{r}, z; \omega)), \tag{4.1}$$

where we retain the notation used in Section 2. However, for convenience, the position vector $\mathbf{r}$ is defined here as the product of $k = 2\pi/\lambda$ by the Cartesian coordinates of the point at which the field is evaluated. Consequently, $(x, y) = \mathbf{r}$ should be considered dimensionless variables.

Let us now introduce the cross-spectral density *matrix* written in the form

$$\hat{W}(\mathbf{r}_1, \mathbf{r}_2, \omega) = \overline{\mathbf{E}^{\dagger}(\mathbf{r}_1, z; \omega)\mathbf{E}(\mathbf{r}_2, z; \omega)}, \tag{4.2}$$

where the overbar denotes an average over an ensemble of realizations, and the dagger indicates the Hermitian conjugate, i.e.,

$$\mathbf{E}^{\dagger} = \begin{pmatrix} E_s^* \\ E_p^* \end{pmatrix}. \tag{4.3}$$

In terms of $\hat{W}$, the so-called Wigner matrix, $\hat{H}$, is defined as [99]

$$\hat{H}(\mathbf{r}, \boldsymbol{\eta}, z) = \frac{1}{k^2} \int\int \hat{W}\left(\mathbf{r} + \frac{\mathbf{s}}{2}, \mathbf{r} - \frac{\mathbf{s}}{2}\right) \exp(\mathrm{i}\mathbf{s} \cdot \boldsymbol{\eta})\, \mathrm{d}\mathbf{s}, \tag{4.4}$$

where $\boldsymbol{\eta} = (u, v)$, with u and v representing propagation angles and $\mathbf{r} = (\mathbf{r}_1 - \mathbf{r}_2)/2$, $\mathbf{s} = \mathbf{r}_1 - \mathbf{r}_2$ as before. For brevity, in Eq. (4.4) and below the dependence on the frequency ω is omitted. No confusion should arise from the fact that the symbol H is also used for the magnetic field, as the Wigner matrix always appears with a caret. Matrix $\hat{H}$ can be expressed in matricial form as follows:

$$\hat{H}(\mathbf{r}, \boldsymbol{\eta}, z) = \begin{pmatrix} h_{ss}(\mathbf{r}, \boldsymbol{\eta}, z) & h_{sp}(\mathbf{r}, \boldsymbol{\eta}, z) \\ h_{ps}(\mathbf{r}, \boldsymbol{\eta}, z) & h_{pp}(\mathbf{r}, \boldsymbol{\eta}, z) \end{pmatrix}, \tag{4.5}$$

where

$$h_{i,j}(\mathbf{r}, \boldsymbol{\eta}, z) = \frac{1}{k^2} \int\int E_i^*\left(\mathbf{r} + \frac{\mathbf{s}}{2}, z\right) E_j\left(\mathbf{r} - \frac{\mathbf{s}}{2}, z\right) \exp(\mathrm{i}\boldsymbol{\eta} \cdot \mathbf{s})\, \mathrm{d}\mathbf{s} \quad i, j = s, p. \tag{4.6}$$

The diagonal elements of this matrix represent the WDF associated to each transverse component of the whole beam (equivalently, the beam emerging from an ideal linear polarizer whose transmission axis is oriented along the s or the p direction). The off-diagonal elements h_{sp} and h_{ps} accounts for the existing correlation between the two components of the field. Comparison with the previous section shows that only the diagonal elements of the Wigner matrix are used in the scalar treatment.

4.2. The Stokes matrices

In terms of matrix $\hat{H}$ the so-called Stokes matrices can be defined in the form [99]

$$\hat{S}_n = \int\int \mathbf{R}^{\mathrm{t}}\mathbf{R}\,\mathrm{Tr}(\hat{\sigma}_n \hat{H}(\mathbf{r}, \boldsymbol{\eta}))\, \mathrm{d}\mathbf{r}\, \mathrm{d}\boldsymbol{\eta}, \quad n = 0, 1, 2, 3, \tag{4.7}$$

where

$$\mathbf{R} \equiv (x, y, u, v) = (\mathbf{r}, \boldsymbol{\eta}) \tag{4.8}$$

is a 1×4 vector, $\hat{\sigma}_0$ is the 2×2 identity matrix and $\hat{\sigma}_1, \hat{\sigma}_2, \hat{\sigma}_3$ are again the Pauli matrices. For convenience, we introduce the following notation:

$$[\alpha\beta]_{ij} \equiv \int\int \alpha\beta h_{ij}(\mathbf{r}, \boldsymbol{\eta}, z)\, \mathrm{d}\mathbf{r}\, \mathrm{d}\boldsymbol{\eta}, \quad i,j = s,p, \;\; \alpha,\beta = x,y,u,v, \tag{4.9}$$

together with

$$[\alpha\beta]_0 \equiv [\alpha\beta]_{ss} + [\alpha\beta]_{pp}, \tag{4.10}$$

$$[\alpha\beta]_1 \equiv [\alpha\beta]_{ss} - [\alpha\beta]_{pp}, \tag{4.11}$$

$$[\alpha\beta]_2 \equiv [\alpha\beta]_{sp} + [\alpha\beta]_{ps}, \tag{4.12}$$

$$[\alpha\beta]_3 \equiv i([\alpha\beta]_{sp} - [\alpha\beta]_{ps}), \quad \alpha,\beta = x,y,u,v, \tag{4.13}$$

where the subscripts 0, 1, 2 and 3 refer to the corresponding Stokes matrices.

As is quite apparent from Eqs. (4.10)–(4.13), Eq. (4.9) is closely related with certain averages of the WDF (second-order moments) defined for scalar fields (see Eq. (3.4)). Moreover, the structure of the quantities $[\alpha\beta]_n$, $n = 0,1,2,3$, resembles the structure of the conventional Stokes parameters. Thus it seems that the present treatment (we refer to it as the Wigner–Stokes formalism) could be a good alternative candidate to describe the transverse spatial behavior of non-uniformly partially-polarized beams. It should be noted that this vectorial formalism reduces to the scalar one for the particular case of uniformly linearly polarized beams. Furthermore, the Stokes parameters can be considered themselves as zero-order moments.

To get deeper insight into the physical meaning of the Stokes matrices, let us write $\hat{S}_0$ in the form

$$\hat{S}_0 = \begin{pmatrix} \hat{W}_0^2 & \hat{\Psi}_0 \\ \hat{\Psi}_0^{\mathrm{t}} & \hat{\Phi}_0^2 \end{pmatrix}, \tag{4.14}$$

where

$$\hat{W}_0^2 = \begin{pmatrix} [x^2]_0 & [xy]_0 \\ [xy_0] & [y^2]_0 \end{pmatrix}, \tag{4.15}$$

$$\hat{\Phi}_0^2 = \begin{pmatrix} [u^2]_0 & [uv]_0 \\ [uv]_0 & [v^2]_0 \end{pmatrix}, \tag{4.16}$$

$$\hat{\Psi}_0 = \begin{pmatrix} [xu]_0 & [xv]_0 \\ [yu]_0 & [yv]_0 \end{pmatrix}, \tag{4.17}$$

are 2×2 matrices that describe

(i) the spatial structure of the beam intensity profile in the near field (matrix $\mathbf{W}_0^2$).
(ii) the divergence of the beam at the far field (matrix $\hat{\Phi}_0^2$).
(iii) the orbital angular moment of the beam (matrix $\hat{\Psi}_0$).
(iv) The averaged curvature radius (elements $[xu]_0, [yv]_0$).

Accordingly, the $\hat{S}_0$ matrix gives, in the vectorial case, a similar information to that provided by the beam matrix ($\hat{M}$) in the scalar case. As a matter of fact, the elements of both matrices are related through the formulae

$$\langle x^2 \rangle = \frac{[x^2]_0}{4\pi^2 k^2 I}, \quad \langle xy \rangle = \frac{[xy]_0}{4\pi^2 k^2 I}, \quad \langle y^2 \rangle = \frac{[y^2]_0}{4\pi^2 k^2 I},$$

$$\langle u^2 \rangle = \frac{[u^2]_0}{4\pi^2 I}, \quad \langle uv \rangle = \frac{[uv]_0}{4\pi^2 I}, \quad \langle v^2 \rangle = \frac{[v^2]_0}{4\pi^2 I},$$

$$\langle xu \rangle = \frac{[xu]_0}{4\pi^2 kI}, \quad \langle xv \rangle = \frac{[xv]_0}{4\pi^2 kI}, \quad \langle yu \rangle = \frac{[yu]_0}{4\pi^2 kI}, \quad \langle yv \rangle = \frac{[yv]_0}{4\pi^2 kI}, \tag{4.18}$$

where

$$I = \frac{1}{4\pi^2} \int \int \mathrm{Tr}\, \hat{H}\, \mathrm{d}\mathbf{r}\, \mathrm{d}\boldsymbol{\eta}, \tag{4.19}$$

is the total intensity of the beam and $\langle \alpha\beta \rangle$, $\alpha, \beta = x, y, u, v$, are the second-order moments introduced for scalar fields in Section 3. We thus conclude that all the spatial parameters defined in the scalar case can be inferred from the knowledge of the $\hat{S}_0$ elements.

As it will be seen below in the paper, the other three matrices, namely, $\hat{S}_1$, $\hat{S}_2$ and $\hat{S}_3$, supply information about the spatial distribution of the polarization state of a beam. For example, for a uniformly totally polarized beam the Stokes matrices take the simple form

$$\hat{S}_1 = (|E_s|^2 - |E_p|^2)\hat{S}_0 = s_1 \hat{S}_0, \tag{4.20}$$

$$\hat{S}_2 = 2\,\mathrm{Re}[E_s^* E_p]\hat{S}_0 = s_2 \hat{S}_0, \tag{4.21}$$

$$\hat{S}_3 = 2\,\mathrm{Im}[E_s^* E_p]\hat{S}_0 = s_3 \hat{S}_0, \tag{4.22}$$

where s_1, s_2 and s_3 may be understood as the Stokes parameters associated to a uniformly polarized plane wave with $s_0 = 1$.

Let us finally remark that all the elements of the four Stokes matrices are measurable quantities. Details of the experimental procedure to determine them will be given in subsequent subsections.

4.3. Second-order classification scheme of partially polarized beams

It can be shown that the diagonal elements of the Stokes matrices fulfill the following inequality:

$$(\mathrm{Tr}\, \hat{S}_0)^2 \geqslant (\mathrm{Tr}\, \hat{S}_1)^2 + (\mathrm{Tr}\, \hat{S}_2)^2 + (\mathrm{Tr}\, \hat{S}_3)^2, \tag{4.23}$$

which closely resembles the well-known inequality satisfied by the Stokes parameters, i.e.,

$$s_0^2 \geqslant s_1^2 + s_2^2 + s_3^2. \tag{4.24}$$

On the basis of condition (4.23), a simple classification scheme of partially polarized beams can be outlined: in fact, any beam should belong to one of the following categories:

(i) *Second-order totally polarized beams*. These are beams fulfilling the equality

$$(\mathrm{Tr}\,\hat{S}_0)^2 = (\mathrm{Tr}\,\hat{S}_1)^2 + (\mathrm{Tr}\,\hat{S}_2)^2 + (\mathrm{Tr}\,\hat{S}_3)^2. \tag{4.25}$$

These kind of fields are the uniformly totally polarized (UTP) beams, whose Cartesian components of the electric field vector are proportional, i.e., $E_s(\mathbf{r}) = \alpha E_p(\mathbf{r})$, where α is a complex number.

(ii) *Second-order non-polarized beams*. These are beams fulfilling

$$\mathrm{Tr}\,\hat{S}_1 = \mathrm{Tr}\,\hat{S}_2 = \mathrm{Tr}\,\hat{S}_3 = 0. \tag{4.26}$$

The locally unpolarized beams ($P(\mathbf{r}) = 0$ everywhere) whose divergences along the s- and p-directions take the same value (i.e., $[\boldsymbol{\eta}^2]_{ss} = [\boldsymbol{\eta}^2]_{pp}$) belong to this type of beams. But this is not the only example. We could also mention, for instance, non-uniformly linearly polarized beams whose polarization plane is oriented along the radial or azimuthal directions and exhibit a radial intensity profile (see Fig. 8).

(iii) *Second-order partially polarized beams*. They are defined through the inequality

$$(\mathrm{Tr}\,\hat{S}_0)^2 > (\mathrm{Tr}\,\hat{S}_1)^2 + (\mathrm{Tr}\,\hat{S}_2)^2 + (\mathrm{Tr}\,\hat{S}_3)^2. \tag{4.27}$$

Beams not included in the above two categories belong to this type.

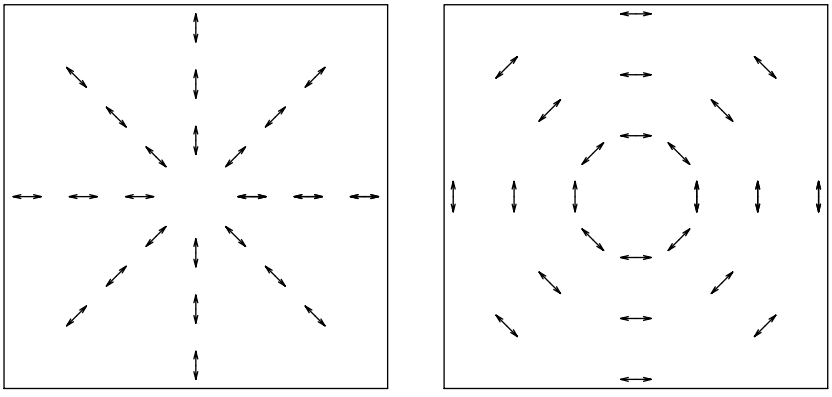

Fig. 8. Radial and azimuthal distributions of the polarization at some plane transverse to the propagation direction of the beam.

4.4. Propagation laws of the Stokes matrices through optical systems

We next study the propagation of the Stokes matrices through optical systems, in order to obtain general enough analytical propagation laws. Here we consider three kinds of systems:

(i) First-order (ABCD) optical systems.
(ii) Spatially-uniform polarization-altering devices.
(iii) Mixed systems (combination of types (i) and (ii)).

(i) *First-order optical (ABCD) systems*

To begin with, let us introduce some preliminary adjustments in the notation. As is well known, first-order optical systems are often represented by a 4×4 simplectic matrix $\hat{\mathscr{S}}$, which can formally be written as

$$\hat{\mathscr{S}} = \begin{pmatrix} \hat{A} & \hat{B} \\ \hat{C} & \hat{D} \end{pmatrix}, \tag{4.28}$$

where $\hat{A}$, $\hat{B}$, $\hat{C}$ and $\hat{D}$ are 2×2 submatrices. In particular, the elements of $\hat{A}$ and $\hat{D}$ are dimensionless, the elements of matrix $\hat{B}$ are expressed in units of length and the elements of $\hat{C}$ are given in units of the inverse of length. However, in the Wigner–Stokes formalism, we use dimensionless position variables. It thus appears to be appropriate to introduce in the calculation a dimensionless ABCD matrix defined as follows:

$$\hat{\mathscr{S}}' = \begin{pmatrix} \hat{A}' & \hat{B}' \\ \hat{C}' & \hat{D}' \end{pmatrix}, \tag{4.29}$$

where $\hat{A}' = \hat{A}$, $\hat{B}' = k\hat{B}$, $\hat{C}' = (1/k)\hat{C}$ and $\hat{D}' = \hat{D}$. It can then be shown that all the relations fulfilled by the former matrix $\hat{\mathscr{S}}$ are still valid for the latter matrix $\hat{\mathscr{S}}'$.

To obtain the propagation law for the Wigner matrix $\hat{H}$ it would suffice to make use of the corresponding law for each Cartesian electric-field component in the scalar case [57,100]. We finally get [101]

$$\hat{H}^{\mathrm{o}}(\mathbf{r}, \boldsymbol{\eta}) = \hat{H}^{\mathrm{i}}(\hat{A}'\mathbf{r} + \hat{B}'\boldsymbol{\eta}, \hat{C}'\mathbf{r} + \hat{D}'\boldsymbol{\eta}), \tag{4.30}$$

where the superscripts i and o denote the input and output planes of the ABCD system, respectively. Taking this into account, it is not difficult to show that the general propagation law for the Stokes matrices reads

$$\hat{S}_n^{\mathrm{o}} = \hat{\mathscr{S}}' \hat{S}_n^{\mathrm{i}} (\hat{\mathscr{S}}')^{\mathrm{t}} \quad n = 0, 1, 2, 3, \tag{4.31}$$

which is formally identical to Eq. (3.11).

Two immediate consequences are inferred from Eq. (4.31):

(a) The Stokes matrices propagate through first-order optical systems independently each other.
(b) According to the second-order classification scheme of light fields given in Section 4.3, there are two kinds of beams that belong to the same type after

propagation through ABCD systems, namely

- Uniformly totally polarized beams.
- Second-order non-polarized beams for which $\hat{S}_1 = \hat{S}_2 = \hat{S}_3 = 0$. This condition is equivalent to say that such beams fulfill

$$[\alpha\beta]_{ss} = [\alpha\beta]_{pp},$$

$$[\alpha\beta]_{sp} = 0, \quad \alpha, \beta = x, y, u, v. \tag{4.32}$$

(ii) *Spatially-uniform polarization-altering (SUPA) systems*

This kind of systems are optical devices whose components modify the polarization state of the light in a uniform way across the transversal section of the beam. They can be described by a Mueller matrix with constant elements. A non-depolarizing deterministic system, represented by its associated Jones matrix, constitutes an example of this class of devices.

It can be shown [99] that the general propagation law for the Stokes matrices reads

$$\hat{S}_n^{\mathrm{o}} = \sum_{m=0}^{3} \mathscr{M}_{nm} \hat{S}_m^{\mathrm{i}}, \quad n, m = 0, 1, 2, 3, \tag{4.33}$$

where $\mathscr{M}_{nm}$ represent the elements of the Mueller matrix. In particular, the propagation law for the $\hat{S}_0$ matrix (which involves the second-order intensity moments of the beam) reduces to

$$\hat{S}_0^{\mathrm{o}} = \sum_{m=0}^{3} \mathscr{M}_{0m} \hat{S}_m^{\mathrm{i}}. \tag{4.34}$$

It is important to note that, unlike that which occurs for ABCD optical systems, the Stokes matrices, in general, do not propagate through SUPA systems independent of each other: in fact, each Stokes matrix at the output of such systems depends, in principle, on the values of the all Stokes matrices of the incident beam.

(iii) *Mixed systems*

This type of systems are optical arrangements composed of a combination of first-order optical systems and SUPA devices cascaded in an arbitrary way. A simple example of such systems is provided by the combination of a polarizer, a free propagation region and a quarter-wave plate. As we will see later, these systems are employed to experimentally determine the elements of the Stokes matrices.

Before deriving the propagation laws of such matrices through mixed systems, let us first enumerate two important properties of these systems:

(a) For any mixed system, the ABCD matrix that represents a first-order optical component commutes with the Mueller matrix associated to a SUPA element. Note, however, that two ABCD matrices, in general, does not commute. The same applies for two Mueller matrices.

(b) All the first-order components of a mixed system, represented by the dimensionless matrices $\hat{\mathscr{S}}_n$, $n = 1, 2, \ldots, N$, can be reduced to an equivalent

first-order optical element whose ABCD matrix, $\hat{\mathscr{S}}^{\mathrm{eq}}$, is given by

$$\hat{\mathscr{S}}^{\mathrm{eq}} = \prod_{n=0}^{N} \hat{\mathscr{S}}_n. \tag{4.35}$$

Analogously, all the SUPA components of a mixed system, represented by the Mueller matrices $\hat{\mathscr{M}}_m$, $m = 1, 2, \ldots, M$, can be reduced to an equivalent SUPA element whose Mueller matrix $\hat{\mathscr{M}}^{\mathrm{eq}}$ is

$$\hat{\mathscr{M}}^{\mathrm{eq}} = \prod_{m=0}^{M} \hat{\mathscr{M}}_m. \tag{4.36}$$

Taking the above properties into account, it is easy to see that the propagation law of the Stokes matrices of a general beam through mixed systems can be written in the form

$$\hat{S}_p^{\mathrm{o}} = \hat{\mathscr{S}}^{\mathrm{eq}} \left(\sum_{q=0}^{3} \hat{\mathscr{M}}_{pq}^{\mathrm{eq}} \hat{S}_q^{\mathrm{i}} \right) (\hat{\mathscr{S}}^{\mathrm{eq}})^{\mathrm{t}}, \quad p, q = 0, 1, 2, 3, \tag{4.37}$$

or, making use of the commutative property,

$$\hat{S}_p^{\mathrm{o}} = \sum_{q=0}^{3} \hat{\mathscr{M}}_{pq}^{\mathrm{eq}} (\hat{\mathscr{S}}^{\mathrm{eq}} \hat{S}_q^{\mathrm{i}}) (\hat{\mathscr{S}}^{\mathrm{eq}})^{\mathrm{t}}, \quad p, q = 0, 1, 2, 3. \tag{4.38}$$

These laws will be next applied to measure the Stokes matrices associated to a beam.

4.5. Experimental procedure to measure the Stokes matrices

The method to determine the Stokes matrices is based on a well-known procedure to find the Stokes parameters. We use a mixed system composed of a quarter-wave plate, a free propagation distance and a linear polarizer. The aim of this system is to establish a relationship between the value of the $\hat{S}_0$ matrix at the plane $z = z_1$ and the values of the Stokes matrices at the plane $z = 0$, which is the plane where we want to measure their values (see Fig. 9).

Several combinations of the above three components exist that allow to infer the Stokes matrices at $z = 0$. Here, we show a specific sequence of measurements that involves six different separate arrangements of these components. The steps are the following:

Step 1: We set a polarizer at the plane $z = z_1$. Its transmission axis makes an angle $\alpha = 0^\circ$ with the s-coordinate axis. Application of the propagation law (4.37) gives

$$\hat{S}_0(z = z_1)|_{\mathrm{step1}} = \hat{\mathscr{S}}'_{z=z_1} [\hat{S}_0(z = 0) + \hat{S}_1(z = 0)] (\hat{\mathscr{S}}'_{z=z_1})^{\mathrm{t}}, \tag{4.39}$$

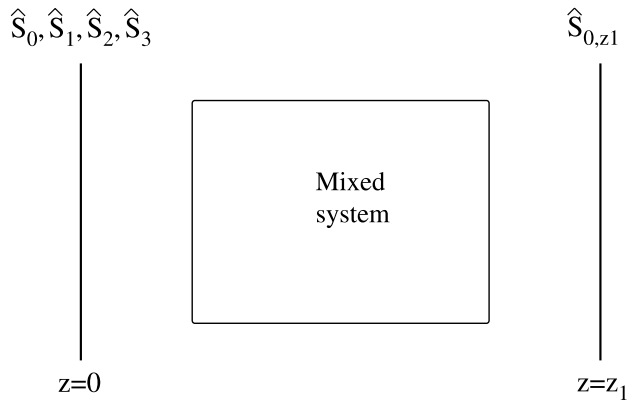

Fig. 9. Schematic and notation used in the experimental procedure employed to measure Stokes matrices.

where $\hat{\mathscr{S}}'_{z=z_1}$ denotes the (modified) ABCD matrix associated to free propagation between planes $z = 0$ and z_1, i.e.,

$$\hat{\mathscr{S}}'_{z=z_1} = \begin{pmatrix} \hat{I} & kz_1\hat{I} \\ 0 & \hat{I} \end{pmatrix}, \tag{4.40}$$

$\hat{I}$ being the 2×2 identity matrix.

Step 2: The same as in step 1 but now with $\alpha = 45^\circ$. In this case the value of $\hat{S}_0$ at the output of the polarizer is given by

$$\hat{S}_0(z = z_1)|_{\text{step2}} = \hat{\mathscr{S}}'_{z=z_1}[\hat{S}_0(z = 0) + \hat{S}_2(z = 0)](\hat{\mathscr{S}}'_{z=z_1})^{\text{t}}. \tag{4.41}$$

Step 3: The same as in step 1 but now with $\alpha = 90^\circ$. Then

$$\hat{S}_0(z = z_1)|_{\text{step3}} = \hat{\mathscr{S}}'_{z=z_1}[\hat{S}_0(z = 0) - \hat{S}_1(z = 0)](\hat{\mathscr{S}}'_{z=z_1})^{\text{t}}. \tag{4.42}$$

Step 4: The same as in step 1 but now with $\alpha = 135^\circ$. In this case

$$\hat{S}_0(z = z_1)|_{\text{step4}} = \hat{\mathscr{S}}'_{z=z_1}[\hat{S}_0(z = 0) - \hat{S}_2(z = 0)](\hat{\mathscr{S}}'_{z=z_1})^{\text{t}}. \tag{4.43}$$

Step 5: The beam propagates successively through a quarter-wave plate (at $z = 0$) whose fast-axis makes an angle 0° with the s-axis, and a polarizer with $\alpha = 45^\circ$ at the plane $z = z_1$. It then follows that

$$\hat{S}_0(z = z_1)|_{\text{step5}} = \hat{\mathscr{S}}'_{z=z_1}[\hat{S}_0(z = 0) - \hat{S}_3(z = 0)](\hat{\mathscr{S}}'_{z=z_1})^{\text{t}}. \tag{4.44}$$

Step 6: The same as in step 5, but now with $\alpha = 135^\circ$. We have

$$\hat{S}_0(z = z_1)|_{\text{step6}} = \hat{\mathscr{S}}'_{z=z_1}[\hat{S}_0(z = 0) + \hat{S}_3(z = 0)](\hat{\mathscr{S}}'_{z=z_1})^{\text{t}}. \tag{4.45}$$

From Eqs. (4.39), (4.41)–(4.45), it can be shown at once that the following relations hold:

$$\hat{S}_0(z = 0) = (\hat{\mathscr{S}}'_{z=z_1})^{-1}[\hat{S}_0(z = z_1)|_{\text{step1}} + \hat{S}_0(z = z_1)|_{\text{step3}}][(\hat{\mathscr{S}}'_{z=z_1})^{\text{t}}]^{-1}, \tag{4.46}$$

$$\hat{S}_1(z = 0) = (\hat{\mathscr{S}}'_{z=z_1})^{-1}[\hat{S}_0(z = z_1)|_{\text{step1}} - \hat{S}_0(z = z_1)|_{\text{step3}}][(\hat{\mathscr{S}}'_{z=z_1})^{\text{t}}]^{-1}, \tag{4.47}$$

$$\hat{S}_2(z=0) = (\hat{\mathscr{S}}'_{z=z_1})^{-1}[\hat{S}_0(z=z_1)|_{\text{step2}} - \hat{S}_0(z=z_1)|_{\text{step4}}][(\hat{\mathscr{S}}'_{z=z_1})^{\text{t}}]^{-1}, \tag{4.48}$$

$$\hat{S}_3(z=0) = (\hat{\mathscr{S}}'_{z=z_1})^{-1}[\hat{S}_0(z=z_1)|_{\text{step6}} - \hat{S}_0(z=z_1)|_{\text{step5}}][(\hat{\mathscr{S}}'_{z=z_1})^{\text{t}}]^{-1}. \tag{4.49}$$

These equations show that the values of $\hat{S}_p(z=0)$, $p=0,1,2,3$, we are looking for can be directly inferred from the values of the Stokes matrix $\hat{S}_0$ at the output plane of the above six configurations. Fortunately, since the elements of $\hat{S}_0$ are connected with the second-order moments (defined in the scalar case) through Eqs. (4.18), our measurement problem would finally reduce to determine such moments according to the procedure described in Section 3.

5. Degrees of polarization

As is well known, the standard degree of polarization, P, of a beam at a certain plane is defined in terms of the Stokes parameters s_n, $n=0,1,2,3$, as follows:

$$P = \frac{(s_1^2 + s_2^2 + s_3^2)^{1/2}}{s_0}. \tag{5.1}$$

Unfortunately, the experimental procedure to determine P involves measurements of the integrated beam intensity over the full detection area. It is then clear that this only makes sense if the light field is assumed to have uniform polarization properties over its cross-sectional region. To obtain a detailed information about the polarization state at each point of the beam profile, a more appropriate parameter is the local degree of polarization, $P(\mathbf{r})$, defined in Section 2. However, two main difficulties appear when we try to handle $P(\mathbf{r})$:

- Actually it is not a parameter or figure of merit, but a point-dependent function.
- The propagation of this function through common optical systems turns out to be very complicated.

To overcome these troubles, in the present section certain new overall parameters are proposed in order to characterize both the degree of polarization and the uniformity of the polarization state across the transverse section of the beam. It will be shown that, in a sense, such parameters provide complementary information about the polarization features of the field. In addition, a measurement procedure is discussed, and some illustrative examples of application are also given.

5.1. Generalized degree of polarization. Definition and properties

Within the framework of the Wigner–Stokes formalism, let us introduce the so-called generalized degree of polarization, defined at a plane transverse to the beam propagation direction in the form [102]

$$P_{\text{G}} = \frac{\sqrt{(\text{Tr}\,\hat{S}_1)^2 + (\text{Tr}\hat{S}_2)^2 + (\text{Tr}\hat{S}_3)^2}}{\text{Tr}\hat{S}_0}. \tag{5.2}$$

As is quite evident from the definition, P_G formally resembles the standard degree of polarization P (cf. Eq. (5.1)). Moreover, this new parameter fulfills similar properties, namely

(i) $0 \leqslant P_G \leqslant 1$. (5.3)

This property is an immediate consequence of Eq. (4.23).

(ii) P_G is independent of the choice of the Cartesian coordinate s- and p-axis. This follows from the fact that P_G is defined in terms of the traces of certain symmetric matrices, which are rotationally invariant.

According to the classification scheme of partially polarized beams introduced in Section 4.3, we conclude at once that

(i) $P_G = 1$ for second-order totally polarized beams,
(ii) $P_G = 0$ for second-order non-polarized beams.

Furthermore, it is easy to see that P_G remains invariant under propagation through ABCD systems for two kind of fields:

(i) Uniformly totally polarized beams.
(ii) Second-order non-polarized beams fulfilling $\hat{S}_1 = \hat{S}_2 = \hat{S}_3 = 0$.

Finally, let us remark that the propagation of P_G is governed by the same law that applies to the Stokes matrices, restricted to their diagonal elements.

5.2. Physical meaning of P_G

To proceed further into the physical meaning of P_G, let us consider a non-uniformly totally-polarized beam whose electric field vector $\mathbf{E}$ at the plane $z = 0$ is given by the Jones vector [102]

$$\mathbf{E}(r) = \begin{pmatrix} E_s(r) \\ E_p(r) \end{pmatrix} = E_0 \exp\left[-\left(\frac{r}{w_0}\right)^2\right] \begin{pmatrix} \cos[f(r)] \\ \sin[f(r)] \end{pmatrix}, \tag{5.4}$$

with

$$f(r) = \frac{\pi}{2} \exp[-(ar)^n], \quad n = 16, \tag{5.5}$$

where E_0 is an amplitude factor, $\mathbf{r}$ denotes the radial polar coordinate, and w_0 and a are constants (w_0 represents the beam size at the waist plane and a^{-1} is a measure of the width of the superGaussian function $f(r)$). Note that the whole beam exhibits a Gaussian intensity profile and, at each point of the beam cross-section, the field is linearly polarized whose azimuth depend on r.

Figs. 10a–c show the spatially distributed polarization of the beam for three different values of the dimensionless product aw_0. As can be seen from these figures, inside the circle whose radius is $\approx a^{-1}$ the beam nearly behaves as a uniformly linearly polarized field with $E_s \approx 0$. However, outside such a circle, the beam remains uniformly polarized but now with negligible p-component. The abrupt transition

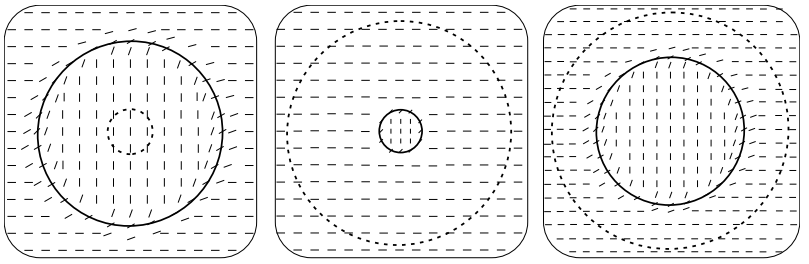

Fig. 10. Spatial distribution of the polarization state of the field $\mathbf{E}(r)$ (Eq. (5.4)) at the transverse plane $z = 0$. The radii of the circles are $1/a$ (continuous line) and w (dashed line). The small segments indicate the local orientation of the linearly polarized field $\mathbf{E}(r)$.

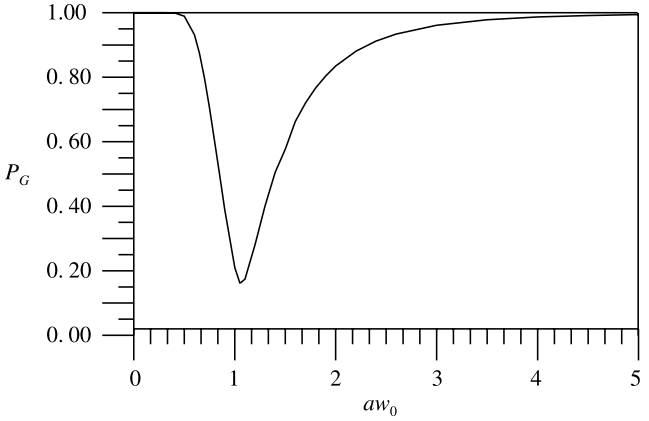

Fig. 11. Generalized degree of polarization P_G versus the dimensionless product aw_0.

between both regions is a consequence of the superGaussian character of function $f(r)$.

In addition, in Fig. 10a ($aw_0 \ll 1$) the beam is linearly p-polarized inside a region where the intensity takes appreciable values (in fact, the significant values of the intensity are concentrated within the solid-line circle). However, in Fig. 10b ($aw_0 \gg 1$) the beam behaves as s-polarized over the whole beam profile except over a small region around its center. Finally, in Fig. 10c ($aw_0 \approx 1$) the global intensities associated to the s- and p-regions are balanced.

The parameter P_G can be computed in terms of the product aw_0. The result is plotted in Fig. 11. We see that P_G is close to unity for the cases shown in Figs. 10a and b, but the value of P_G drastically reduces ($P_G < 0.3$) when aw_0 approaches 1 (Fig. 10c).

It can then be concluded that, for non-uniformly totally polarized beams, P_G represents a measure of the uniformity of the polarization state over the regions of the beam cross-section where the intensity is not negligible. Thus, values of P_G close

to unity means that the beam essentially behaves as uniformly polarized, at least over the transverse region where the intensity is significant. The value of $P_G \approx 0$ would imply, however, the lack of an overall definite polarization state over such peak intensity area.

5.3. Experimental determination of P_G

The generalized degree of polarization P_G can be measured in several ways. Here we propose an experimental procedure based on the six-step method explained in Section 4.5 to measure the Stokes matrices. In the present case we should determine the global intensity (integrated across the beam profile) and two second-order moments, namely, the beam size and the beam divergence, for several orientations of a polarizer and a quarter-wave plate. The observation plane should remain unchanged during the procedure.

Application of the propagation law of the Stokes matrices leads to the following expressions [103]:

$$\mathrm{Tr}\,\hat{S}_0 = \frac{4\pi^2}{T_1 + T_2}[I_{\mathrm{step1}}(k^2 \langle r^2 \rangle_{\mathrm{step1}} + \langle \eta^2 \rangle_{\mathrm{step1}}) + I_{\mathrm{step3}}(k^2 \langle r^2 \rangle_{\mathrm{step3}} + \langle \eta^2 \rangle_{\mathrm{step3}})], \tag{5.6}$$

$$\mathrm{Tr}\,\hat{S}_1 = \frac{4\pi^2}{T_1 - T_2}[I_{\mathrm{step1}}(k^2 \langle r^2 \rangle_{\mathrm{step1}} + \langle \eta^2 \rangle_{\mathrm{step1}}) - I_{\mathrm{step3}}(k^2 \langle r^2 \rangle_{\mathrm{step3}} + \langle \eta^2 \rangle_{\mathrm{step3}})], \tag{5.7}$$

$$\mathrm{Tr}\,\hat{S}_2 = \frac{4\pi^2}{T_1 - T_2}[I_{\mathrm{step2}}(k^2 \langle r^2 \rangle_{\mathrm{step2}} + \langle \eta^2 \rangle_{\mathrm{step2}}) - I_{\mathrm{step4}}(k^2 \langle r^2 \rangle_{\mathrm{step4}} + \langle \eta^2 \rangle_{\mathrm{step4}})], \tag{5.8}$$

$$\mathrm{Tr}\,\hat{S}_3 = \frac{4\pi^2}{T_3(T_1 - T_2)}[I_{\mathrm{step5}}(k^2 \langle r^2 \rangle_{\mathrm{step5}} + \langle \eta^2 \rangle_{\mathrm{step5}}) - I_{\mathrm{step6}}(k^2 \langle r^2 \rangle_{\mathrm{step6}} + \langle \eta^2 \rangle_{\mathrm{step6}})], \tag{5.9}$$

where we have included the coefficients T_1 and T_2 that represent the major and minor principal transmittances of the (non-ideal) polarizer, T_3 is the transmittance of the retarder plate and the symbol I refers to the global intensity associated to each step. In the above equations all the magnitudes that appears in the right-hand side should be considered as experimental data, from which the value of P_G can be inferred at once.

It should be noted that this method could be shortened by excluding steps 4 and 6, in which the polarizer is oriented at $\alpha = 135^\circ$. However, this possibility has been rejected since, in practice, it would involve higher experimental errors [103].

Although the procedure just shown is conceptually simple, some care, however, is required to implement the experiment because the optical components (polarization-altering devices and photodetector array) are not ideal and may exhibit certain harmful effects. To illustrate this let us consider the beam emitted by a He–Ne laser source Spectra Physics 117A (intensity and frequency-stabilized mode), linearly (> 1000:1) and uniformly polarized according to the manufacturer specifications. We have chosen this kind of beam because it allows to check the expected theoretical value $P_G = 1$, and the possible error sources are simpler to detect.

The power measurements were carried out using a powermeter (Newport model 815) and the second-order moments were determined by means of a CCD camera Pulnix TM765 in combination with a laser beam analyzer Spiricon LBA-300PC (see Fig. 12). We used a linear polarizer whose extinction ratio is $T_1/T_2 = 250$ and a quarter-wave plate with a transmittance $T_3 = 0.98$. The measured divergences resulted to be much smaller than the terms associated to the widths $k^2\langle r^2\rangle$, so that they can be neglected.

Special attention was taken to align the system in order that the beam crosses through the center of both the polarizer and the retarder plate. In such a case, when these components rotate, the influence of their spatial inhomogeneities on the global intensity will be strongly reduced.

In our six-step method, at the output of each configuration three measurements were taken, each of them representing the result of the simultaneous automatic average of 32 images carried out by the beam analyzer. The mean values were taken as experimental data.

The experimental procedure was carried out for different orientations of the Cartesian reference system. Fig. 13 shows the dependence of P_G on θ_R, where θ_R denotes the angle that forms the polarization plane of the initial beam (fixed all along the experiment) and the s-axis, which is parallel to the transmission axis of the polarizer when $\alpha = 0^\circ$. Note that, in an ideal configuration, P_G should be independent of θ_R because P_G is invariant under rotation of the coordinate system.

The experimental values show a discrepancy of 1% with regard to the expected value. This deviation is mainly due to the distortion that the polarizer produces on the beam intensity profile. This effect is illustrated in Fig. 14. Although at the entrance plane of the polarizer the beam cross-section is completely circular, however, at the output the polarizer has generated an astigmatic distortion, and the profile is no longer circularly symmetric.

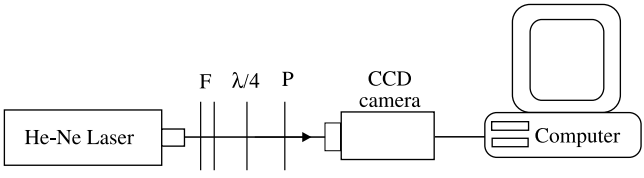

Fig. 12. Experimental setup used to measure P_G. F represents neutral filters, $\lambda/4$ denotes the quarter-wave plate and P is a linear polarizer.

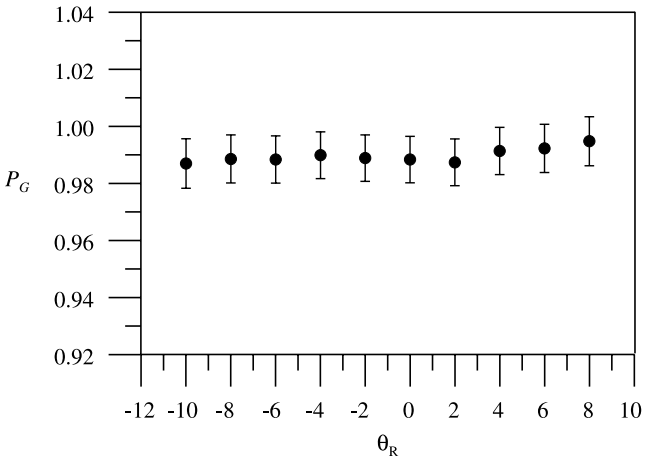

Fig. 13. Generalized degree of polarization in terms of θ_R (in degrees): experimental results (for details, see text).

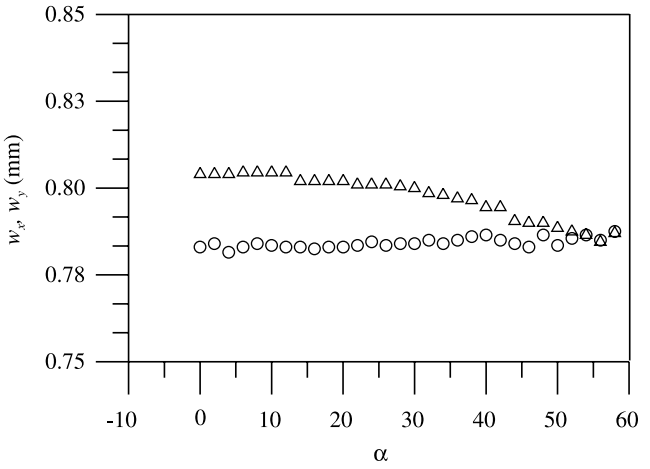

Fig. 14. Beam width along two orthogonal axis (w_x (circles) and w_y (triangles)) at the output of the polarizer in terms of the angle α (in degrees) that forms the transmission axis of the polarizer with the azimuth of the incident linearly polarized field: in general, $w_x \neq w_y$ (astigmatic beam), except for the interval $\alpha \in [53°, 58°]$, where the beam profile remains circular.

The error bars in Fig. 13 also arise from the angular precision of the polarizer and retarder-plate holders (1°) and from the measurement process of the total intensity and of the beam widths: although, theoretically, the beam size of a uniformly polarized field should not change after crossing through an ideal polarizer, however, in practice, the total intensity reduction produced by the polarizer affects the experimental beam width due to the influence of background and offset noises.

Next we will apply the measurement procedure described before the study of active media in solid-state laser resonators. We will see that P_G could be a useful tool to get information about certain parameters of the system.

5.4. Generalized degree of polarization of beams emerging from an optically pumped Nd:YAG rod

As is well known, the active medium in high-power solid-state laser cavities is subjected to thermal processes generated by both absorption of radiation and cooling. Inside such a material (for example, cylindrical rod in Nd:YAG lasers), these thermal effects give rise to a change in the temperature, which becomes a function of the radial polar coordinate r (assuming that the heat conductivity is constant and the laser rod is homogeneously pumped). In addition, birefringent mechanical strains are also induced by the temperature gradient.

Let us now focus our attention on high-power Nd:YAG lasers. In such a case, the thermal processes, in turn, produce changes in the refractive index of the active medium: the refractive index exhibits a parabolic dependence on r leading to the laser rod to behave as a thin lens (thermal lens). Moreover, the rod becomes birefringent with two different values of the refractive index, n_r and n_ϕ, associated to light polarized along radial and azimuthal directions, respectively [104]

$$n_r(r) = n_0\left(1 - \frac{\alpha_r}{2}r^2\right), \tag{5.10}$$

$$n_\phi(r) = n_0\left(1 - \frac{\alpha_\phi}{2}r^2\right), \tag{5.11}$$

n_0 being the refractive index at the center of the rod, and

$$\alpha_r = \frac{P_a}{\pi L R^2}\frac{1}{K_t}\left(\frac{1}{2n_0}\frac{\partial n}{\partial T} + n_0^2\alpha C_r\right), \tag{5.12}$$

$$\alpha_\phi = \frac{P_a}{\pi L R^2}\frac{1}{K_t}\left(\frac{1}{2n_0}\frac{\partial n}{\partial T} + n_0^2\alpha C_\phi\right), \tag{5.13}$$

where P_a is the total power absorbed by the rod, R and L denote, respectively, the radius and the length of the rod, K_t is the thermal conductivity, α is the thermal expansion coefficient, C_r and C_ϕ are the photoelastic coefficients associated to the radial and azimuthal components, respectively, and $\partial n/\partial T$ represents the variation of the refractive index with the temperature.

Let us assume that the cylindrical rod can be considered as a phase plate in such a way that the beam diameter does not change, in a significant way, when the beam propagates through the rod. This approach will be accurate for well-collimated beams or, equivalently, for small values of the ratio L/z_R, where z_R is the Rayleigh length of the beam. In this case, the birefringent medium may be represented by the

following Jones matrix (referred to the Cartesian s- and p-axis):

$$\hat{J} = \begin{pmatrix} J_{ss}(r,\theta) & J_{sp}(r,\theta) \\ J_{sp}(r,\theta) & J_{pp}(r,\theta) \end{pmatrix}, \tag{5.14}$$

with

$$J_{ss}(r,\theta) = \mathrm{e}^{-\mathrm{i}kLn_r(r)}\cos^2\theta + \mathrm{e}^{-\mathrm{i}kLn_\phi(r)}\sin^2\theta, \tag{5.15}$$

$$J_{sp}(r,\theta) = [\mathrm{e}^{-\mathrm{i}kLn_\phi(r)} - \mathrm{e}^{-\mathrm{i}kLn_r(r)}]\sin\theta\cos\theta, \tag{5.16}$$

$$J_{pp}(r,\theta) = \mathrm{e}^{-\mathrm{i}kLn_r(r)}\sin^2\theta + \mathrm{e}^{-\mathrm{i}kLn_\phi(r)}\cos^2\theta, \tag{5.17}$$

where the angle θ is represented in Fig. 15.

Since the elements of matrix $\hat{J}$ depend on the variables r and θ, the active medium would modify, in general, the polarization state of the input beam in a spatially non-uniform way. Note, however, that incident beams with radial or azimuthal linear polarization do not alter their polarization state after crossing the rod.

Here we consider a linearly polarized rotationally symmetric Gaussian beam whose waist coincides with the entrance plane of the active medium. The amplitude of the electric field vector associated to such beam can then be represented

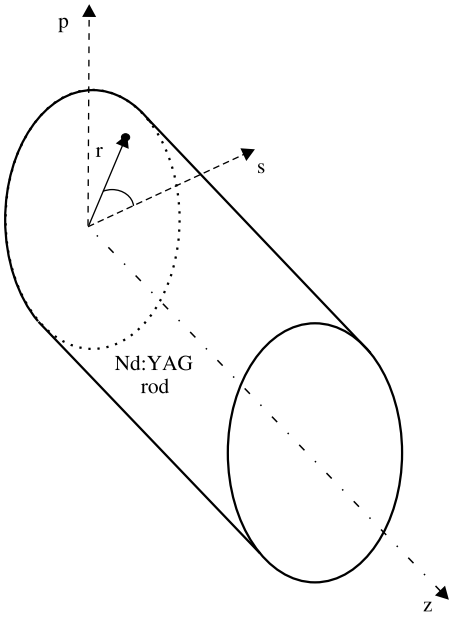

Fig. 15. Geometry and notation used to write the matrix $\hat{J}$ (Eq. (5.14)): r and θ are polar coordinates at a plane perpendicular to the rod axis z.

by the Jones vector

$$\mathbf{E}(r,\theta) = E_0 \exp\left(-\frac{r^2}{w_0^2}\right)\begin{pmatrix}1\\0\end{pmatrix}, \tag{5.18}$$

where E_0 and w_0 are constants.

By assuming the rod wide enough to neglect the border effects (diffraction and gain saturation effects are also ignored), the *s*- and *p*-components of the beam at the output plane of the rod are obtained by applying the Jones matrix $\hat{J}$ to $\mathbf{E}(r,\theta)$. Accordingly, the components of the output field are

$$E_s(r,\theta) = E_0[\mathrm{e}^{-\mathrm{i}kLn_r(r)}\cos^2\theta + \mathrm{e}^{-\mathrm{i}kLn_\phi(r)}\sin^2\theta]\exp\left(-\frac{r^2}{w_0^2}\right), \tag{5.19}$$

$$E_p(r,\theta) = E_0\sin\theta\cos\theta[\mathrm{e}^{-\mathrm{i}kLn_\phi(r)} - \mathrm{e}^{-\mathrm{i}kLn_r(r)}]\exp\left(-\frac{r^2}{w_0^2}\right). \tag{5.20}$$

We see that the polarization state of the output field is not uniform across the beam section. The intensity of each field component is

$$I_s = \frac{I}{4}\left(3 + \frac{1}{1+\beta}\right), \tag{5.21}$$

$$I_p = \frac{I}{4}\left(\frac{\beta}{1+\beta}\right), \tag{5.22}$$

where $I = \pi w_0^2/2$ and

$$\beta = \left(\frac{n_0^3\alpha(C_r - C_\phi)}{2\lambda K_\mathrm{t}}\frac{w_0^2}{R^2}P_\mathrm{a}\right)^2. \tag{5.23}$$

It is important to note that β is directly related to the pumping power $P_\mathrm{p} = P_\mathrm{a}/\eta$, where η (<1) represents the ratio $P_\mathrm{a}/P_\mathrm{p}$. Moreover, in terms of β the second-order moments associated to each field component read

$$\langle r^2\rangle_s = \frac{I}{4I_s}\frac{w_0^2}{2}\left[3 + \frac{1-\beta}{(1+\beta)^2}\right], \tag{5.24}$$

$$\langle r^2\rangle_p = \frac{I}{4I_p}\frac{w_0^2}{2}\frac{\beta(3+\beta)}{(1+\beta)^2}, \tag{5.25}$$

$$\langle \mathbf{r}\cdot\boldsymbol{\eta}\rangle_s = \frac{I}{4I_s}\frac{w_0^2}{2}\frac{(\alpha_r+\alpha_\phi)Ln_\mathrm{o}}{2}\left[3 + \frac{1-\beta}{(1+\beta)^2}\right], \tag{5.26}$$

$$\langle \mathbf{r}\cdot\boldsymbol{\eta}\rangle_p = \frac{I}{4I_s}\frac{w_0^2}{2}\frac{(\alpha_r+\alpha_\phi)Ln_\mathrm{o}}{2}\frac{\beta(3+\beta)}{(1+\beta)^2}, \tag{5.27}$$

$$\langle \eta^2 \rangle_s = \frac{I}{2I_s}\frac{w_0^2}{2}\frac{(\alpha_r^2+\alpha_\phi^2)L^2 n_o^2}{4}\left[3+\frac{1-\beta}{(1+\beta)^2}\right] + \frac{\pi}{4k^2 I_s}\left[5-\frac{1+3\beta}{(1+\beta)^2}+2\ln(1+\beta)\right], \tag{5.28}$$

$$\langle \eta^2 \rangle_p = \frac{I}{2I_p}\frac{w_0^2}{2}\frac{(\alpha_r^2+\alpha_\phi^2)L^2 n_o^2}{4}\frac{\beta(3+\beta)}{(1+\beta)^2} + \frac{\pi}{4k^2 I_s}\left[\frac{\beta(1-\beta)}{(1+\beta)^2}+2\ln(1+\beta)\right]. \tag{5.29}$$

These equations give, in a simple analytical way, the influence of the pumping power on the spatial structure of the laser beam (transverse size and divergence). In addition, making use of the analytical expressions for the field components, we can obtain the value of the generalized degree of polarization P_G of the output beam. After lengthy but straightforward calculations we find the simple expression

$$P_G = \frac{1}{2}\left[1+\frac{1-\beta}{(1+\beta)^2}\right]. \tag{5.30}$$

We thus see that a one-to-one correspondence exists between P_G and β. Consequently, for our incident Gaussian beam, determination of the parameter P_G would provide the value of β. It should be remarked that β contains information about the optical characteristics of the material, the beam size and the energy supplied to the medium.

The experimental setup used to measure P_G is shown in Fig. 16. The physical constants of the Nd:YAG rod are $L = 17$ cm, $R = 0.32$ cm, $n_o = 1.82$, $\alpha = 7.9 \times 10^{-6}$ K^{-1}, $K_t = 0.13$ W K^{-1} cm^{-1}, $\lambda = 632.8$ nm, $C_r = 0.017$ and $C_\phi = -0.0025$. In this figure F denotes neutral filters employed to attenuate the beam intensity, P1 represents a polarizer that controls the azimuth of the incident beam, M indicates the presence of a magnifier 3× that increases the beam size, A1 and A2 are two apertures to avoid that the light coming from the pumping lamps enter inside the detector and finally $\lambda/4$ and P2 symbolize the quarter-wave plate and the polarizer, respectively, that are used in the six-step method to determine the traces of the Stokes matrices.

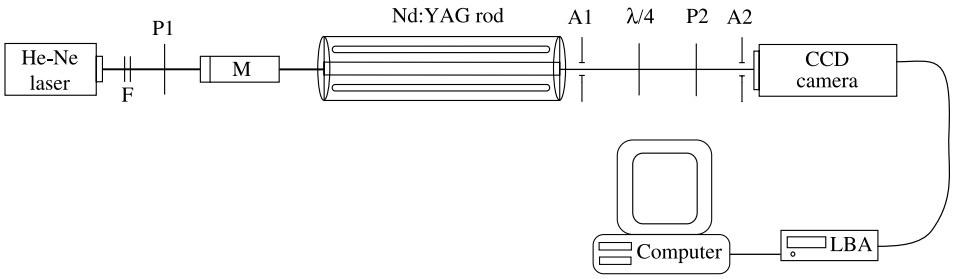

Fig. 16. Experimental setup used to measure P_G of an initial Gaussian beam after crossing a birefringent optically pumped Nd:YAG rod.

Fig. 17 illustrates the non-uniform spatial structure of the polarization state of the beam emerging from the rod. For comparatives purposes, it is also shown in the figure the uniformly distributed polarization state of the incident linearly polarized Gaussian beam. Fig. 18 plots P_G as a function of β. The dots represent the experimental values and the continuous line is the theoretical curve (Eq. (5.30)) that best fits the measured data. No experimental point has been represented in the central region of the curve because the beam size at the observation plane is not large enough to allow the accurate measurement of its width. The error bars are smaller for low values of the pumping power because under such conditions only a negligible amount of light coming from the pumping lamps goes into the CCD camera. This allows to increase the accuracy of the measurement. From the fitting process we set for the ratio P_a/P_p the value $\eta = 0.05$.

Fig. 18 also shows that the beam essentially behaves as a uniformly polarized field across its transversal section for low values of β. However, as β increases, the value of P_G reduces: pumping produces non-uniform optical anisotropies inside the rod

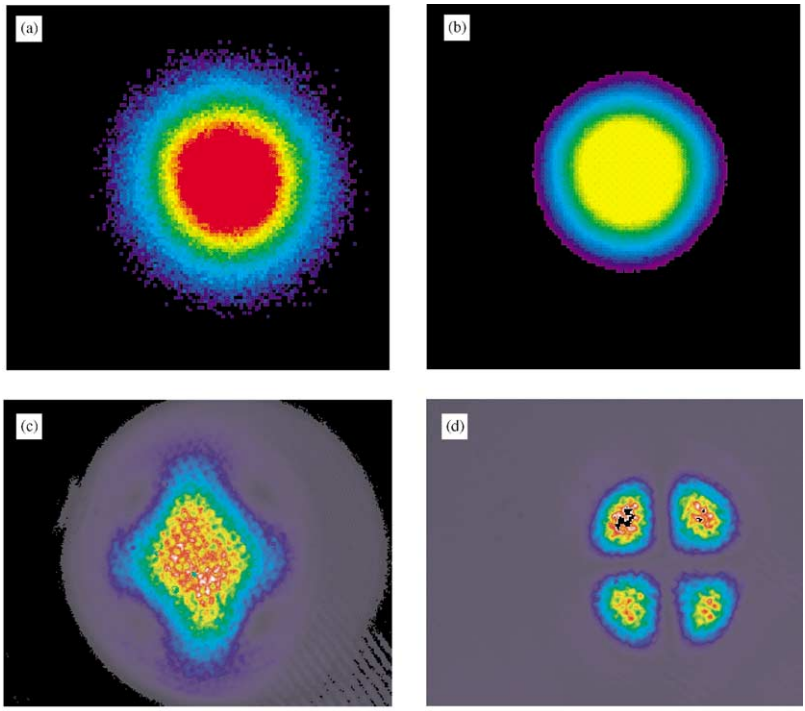

Fig. 17. Transverse intensity profiles (pseudocoloured) of two laser beams after crossing a polarizer for two orientations of its transmission axis. (a) and (b) correspond to the incident rotationally symmetric Gaussian beam used in the experiment mentioned in the text. The spatial symmetry is the same for both orientations. (c) and (d) refer to the beam at the output of a birefringent optically pumped Nd:YAG rod. The spatial structure of the beam drastically changes when the polarizer rotates. This indicates a non-uniformly distributed polarization state across the beam profile.

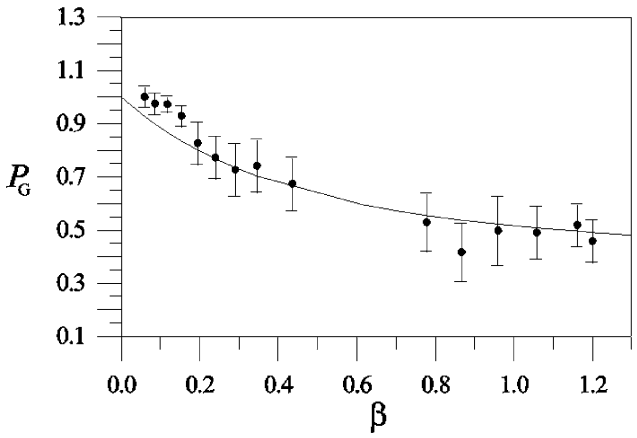

Fig. 18. P_G in terms of β. The dots represent the experimental data and the continuous line is the theoretical curve (cf. Eq. (5.30)) that best fits the experimental values.

within the central regions crossed by the beam. This leads to a non-uniform polarization distribution. Finally, P_G reaches a quasi-asymptotic behavior for high pumping power, which implies that depolarization is not complete. The same conclusion was also obtained by other authors studying a similar system [105].

5.5. Weighted degree of polarization

As it was pointed out before, the generalized degree of polarization P_G could be used to globally describe the spatial distribution of the polarization state of non-uniformly totally polarized beams. However, without any additional knowledge no conclusion could be obtained from a given value of P_G concerning whether the field is actually partially polarized or shows a spatial dependence of the polarization over the beam cross-section. In order to distinguish between both possibilities, we next introduce two new measurable overall parameters, which, in a sense, may be considered as complementary to P_G.

We define the so-called weighted degree of polarization as [106]

$$\tilde{P} = \frac{\int\int I(\mathbf{r})P(\mathbf{r})\,\mathrm{d}\mathbf{r}}{\int\int I(\mathbf{r})\,\mathrm{d}\mathbf{r}}, \tag{5.31}$$

where $I(\mathbf{r})$ and $P(\mathbf{r})$ denote, respectively, the intensity and the local degree of polarization of the field at each point of the beam cross-section at the observation plane.

As is quite apparent from the definition, $\tilde{P}$ essentially represents the local degree of polarization averaged (and normalized) over those regions of the wavefront where the intensity is significant. The existence of the factor $I(\mathbf{r})$ inside the integral in Eq. (5.31) is particularly useful to measure $\tilde{P}$ with accuracy, because it reduces the influence of the tales of the beam profile, thus decreasing certain harmful effects such as small signal-to-noise ratio, background, camera offset, etc. It should also be noted

that, in general, $\tilde{P}$ is not invariant under propagation through ABCD optical systems.

The dispersion of the values of $\tilde{P}$ across the beam section can be evaluated in a simple way by means of the following parameter [106]:

$$\tilde{\sigma}_p^2 = \frac{\int\int I(\mathbf{r})[P(\mathbf{r}) - \tilde{P}]^2 \, \mathrm{d}\mathbf{r}}{\int\int I(\mathbf{r}) \, \mathrm{d}\mathbf{r}}, \tag{5.32}$$

which should be considered as the variance of $P(\mathbf{r})$ (the intensity $I(\mathbf{r})$ behaves as a density function). This parameter globally characterizes the uniformity of the local degree of polarization over the transversal section of the beam.

The above two parameters satisfy the following inequalities:

$$0 \leqslant \tilde{P} \leqslant 1, \tag{5.33}$$

$$0 \leqslant \tilde{\sigma}_p \leqslant 1/2. \tag{5.34}$$

Those fields whose parameter $\tilde{P}$ approaches 1 could be considered as (nearly) totally polarized in the region where the intensity is not negligible. When $\tilde{P}$ vanishes, the field is non-polarized throughout the beam profile. Of course, for beams whose polarization state is uniform $\tilde{\sigma}_p^2 = 0$. Intermediate values of $\tilde{P}$ would indicate that the beam is partially polarized.

Parameters $\tilde{P}$ and $\tilde{\sigma}_p^2$ are, in a sense, complementary to P_G. To illustrate this, let us consider, for instance, a radially polarized beam, whose polarization state is linear and oriented along radial lines from the beam axis. Such beams have been synthesized, in practice, by using interferometric methods and concentric-circular-grating surface semiconductor lasers [20,22,23]. For these fields $\tilde{P} = 1$ and $\tilde{\sigma}_p^2 = 0$, which are identical to the values associated to uniformly totally polarized beams. To distinguish between both kind of beams we can use the parameter P_G: in fact, P_G equals zero for radially polarized fields but reaches its maximum value $P_\mathrm{G} = 1$ for uniformly totally polarized beams.

In conclusion, the triad of parameters P_G, $\tilde{P}$ and $\tilde{\sigma}_p^2$ provide an overall parametric characterization of the spatial distribution of the polarization state over the whole beam profile. On the basis of these three figures of merit, a rough but rather simple classification scheme of general partially polarized beams may formally be proposed. Fig. 19 shows the sequence we have to follow to classify a beam according to this scheme (for example, the values $\tilde{\sigma}_p^2 = 0$, $\tilde{P} = 1$, $P_\mathrm{G} < 1$ would indicate the presence of a non-uniformly totally polarized beam). In addition, the values of the parameters $\tilde{P}$ and $\tilde{\sigma}_p^2$ could also reveal a number of specific characteristics of certain fields. We will next illustrate this point by means of an example.

5.6. Application to partially polarized Gaussian Schell-model (PGSM) sources

Gaussian Schell-model (GSM) sources have been extensively studied in the scalar case [107]. This kind of beams provides a good model to represent partially polarized sources as well as some types of multimode lasers. These scalar fields are characterized by their cross-spectral density function, which at a certain plane has

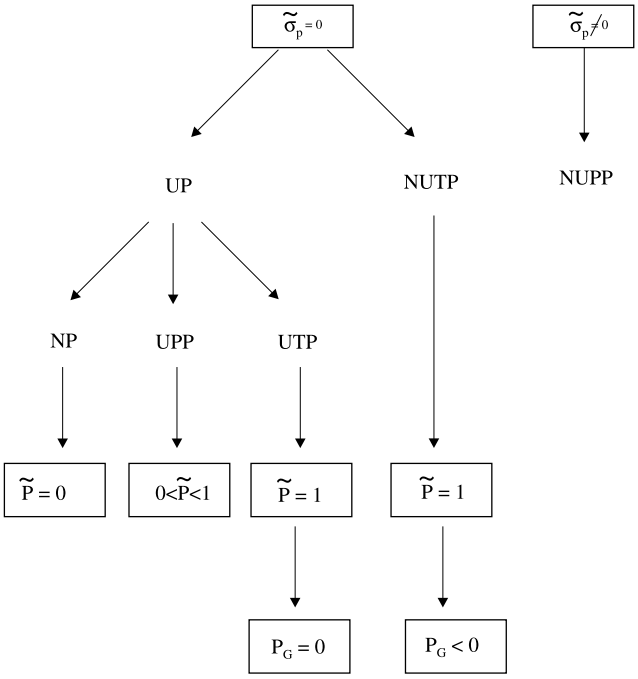

Fig. 19. Classification scheme of partially polarized beams based on the parameters P_G, $\tilde{P}$ and $\tilde{\sigma}_p$. The acronyms refer to the following type of fields: UP (uniformly polarized beams); NUTP (non-uniformly totally polarized beams); NUPP (non-uniformly partially polarized beams); NP (non-polarized beams); UPP (uniformly partially polarized beams); UTP (uniformly totally polarized beams).

the form

$$W(\mathbf{r}_1, \mathbf{r}_2) = I_0 \exp\left[-\frac{r_1^2 + r_2^2}{4\sigma_I^2}\right] \exp\left[-\frac{(\mathbf{r}_1 - \mathbf{r}_2)^2}{2\sigma_\mu^2}\right], \tag{5.35}$$

where $\mathbf{r}_1$ and $\mathbf{r}_2$ are two-dimensional position vectors, I_0 represents the intensity at the center of the beam (z-axis), σ_I^2 is proportional to the width of the beam profile and σ_μ^2 is proportional to the transverse coherence length. It is clear from the definition that both the intensity profile and the degree of coherence of a GSM source are Gaussian. Furthermore, in the scalar treatment, GSM fields are assumed to be uniformly totally polarized.

When one considers the vectorial case, that is, we handle partially polarized Gaussian Schell-model (PGSM) sources, the fields should be characterized by means of the beam coherence-matrix (see Section 2.3), whose elements read at plane $z = 0$ [33]

$$G_{ij}(\mathbf{r}_1, \mathbf{r}_2, z = 0) = (I_0)_{ij} \exp\left[-\frac{r_1^2 + r_2^2}{4\sigma_{I_{ij}}^2}\right] \exp\left[-\frac{(\mathbf{r}_1 - \mathbf{r}_2)^2}{2\sigma_{\mu_{ij}}^2}\right], \quad i,j = s,p, \tag{5.36}$$

where $\sigma_{I_{ij}}^2$ and $\sigma_{\mu_{ij}}^2$ and $(I_0)_{ij}$ are positive constants. In particular, $\sigma_{I_{ii}}^2$, $\sigma_{\mu_{ii}}^2$ and $(I_0)_{ii}$, $i = s, p$, are related, respectively, with the beam size, the transverse coherence length and the beam intensity associated to each field component, and $(I_0)_{sp}$ (also $(I_0)_{ps}$) accounts for a constant phase shift between the s and p-components of the field. Since such a phase could be easily canceled out by means of a suitable phase plate, for simplicity, the argument of $(I_0)_{sp}$ will be set equal to zero from now on. Furthermore, the non-negativeness property of the BCP matrix implies that $I_{sp}^2 \leqslant I_{ss} I_{pp}$.

Here we are interested on the establishment of some relationship between the weighted degree of polarization and a certain type of PGSM sources, namely, those fields whose associated BCP matrix is written in the form

$$\hat{G}(\mathbf{r}_1, \mathbf{r}_2, z = 0) = I_0 \exp\left[-\frac{r_1^2 + r_2^2}{4\sigma_I}\right] \begin{pmatrix} \exp\left[-\dfrac{(\mathbf{r}_1 - \mathbf{r}_2)^2}{2\sigma_{\mu_{ss}}^2}\right] & \chi \exp\left[-\dfrac{(\mathbf{r}_1 - \mathbf{r}_2)^2}{2\sigma_{\mu_{sp}}^2}\right] \\ \chi \exp\left[-\dfrac{(\mathbf{r}_1 - \mathbf{r}_2)^2}{2\sigma_{\mu_{sp}}^2}\right] & \exp\left[-\dfrac{(\mathbf{r}_1 - \mathbf{r}_2)^2}{2\sigma_{\mu_{ss}}^2}\right] \end{pmatrix}, \tag{5.37}$$

where χ is a positive number < 1. It is important to note that the beams generated by this kind of sources cannot be distinguished from ordinary GSM fields when polarization measurements are disregarded (i.e., when no anisotropic element is inserted on the beam path). The propagation of these beams in the paraxial regime can be analyzed from the application to each matrix element of the usual formulae, extensively employed in the scalar case [108]. In addition, for these particular beams, the local degree of polarization $P(\mathbf{r})$ turns out to be a Gaussian function of the radial polar variable r at the far field [33,109]. This remarkable analytical behavior suggests to handle the parameters $\tilde{P}$ and $\tilde{\sigma}_p^2$ at the far field too. After some calculations, we finally obtain the simple expressions

$$\tilde{P}^{(\infty)} = \chi, \tag{5.38}$$

$$\tilde{\sigma}_p^{(\infty)} = \chi \left\{ \frac{\gamma^2}{(2\gamma - 1)} - 1 \right\}^{1/2}, \tag{5.39}$$

where γ approaches the ratio $\sigma_{\mu_{sp}}^2 / \sigma_{\mu_{ss}}^2$ at the far field, and fulfills

$$1 \leqslant \gamma \leqslant \chi^{-1}. \tag{5.40}$$

We thus see that the parameters $\tilde{P}^{(\infty)}$ and $\tilde{\sigma}_p^{(\infty)}$ may be used to determine the constants χ and γ that define and characterize this class of PGSM sources.

Of course, this is only a simple analytical example to illustrate the possible applications of the weighted degree of polarization. It remains to find further relationships between these figures of merit and the structure of partially polarized fields. This constitutes, at present, an interesting research line, which should be explored in the future.

5.7. Measurement of $\tilde{P}$ and $\tilde{\sigma}_p$

To measure $\tilde{P}$ and $\tilde{\sigma}_p^2$ we have to obtain both the local degree of polarization $P(\mathbf{r})$ and the beam intensity at each point of the wavefront, $I(\mathbf{r})$. To do this, a six-step procedure similar to that used to obtain the Stokes parameters may be used (see also Section 4.5). Here a CCD array captures the beam intensity at each point of the observation plane.

From the six measured values of the intensity for the different configurations of the polarizer and the quarter-wave plate, the point-dependent Stokes parameters can be computed as follows:

$$s_0(\mathbf{r}) = I(\mathbf{r})_{\text{step1}} + I(\mathbf{r})_{\text{step3}}, \tag{5.41}$$

$$s_1(\mathbf{r}) = I(\mathbf{r})_{\text{step1}} - I(\mathbf{r})_{\text{step3}}, \tag{5.42}$$

$$s_2(\mathbf{r}) = I(\mathbf{r})_{\text{step4}} - I(\mathbf{r})_{\text{step2}}, \tag{5.43}$$

$$s_3(\mathbf{r}) = I(\mathbf{r})_{\text{step6}} - I(\mathbf{r})_{\text{step5}}. \tag{5.44}$$

The function $P(\mathbf{r})$ is then calculated making use of Eq. (2.41). The weighted degree of polarization is finally obtained from the formula

$$\tilde{P} = \frac{\sum_{n,m} I(\mathbf{r})_{n,m} P(\mathbf{r})_{n,m}}{\sum_{n,m} I(\mathbf{r})_{n,m}}, \tag{5.45}$$

where the subscripts n and m refer to the pixel that contributes to the calculus. In the same way we have

$$\tilde{\sigma}_p^2 = \frac{\sum_{n,m} I(\mathbf{r})_{n,m} [P_{n,m}(\mathbf{r}) - \tilde{P}]^2}{\sum_{n,m} I(\mathbf{r})_{n,m}}. \tag{5.46}$$

To illustrate the experimental procedure we next present some results concerning the measurements of $\tilde{P}$ and $\tilde{\sigma}_p^2$ for two kind of laser beams, namely

(i) A uniformly linearly polarized Gaussian beam, emitted by a He–Ne laser cavity.
(ii) A non-uniformly partially polarized beam (see Fig. 20) generated by a diode laser LDM-135 ($\lambda = 670$ nm).

Fig. 20

Both cases employ a CCD camera (Pulnix TM-765) with a 8.8 mm × 6.6 mm sensitive area (756 pixels in the horizontal axis and 581 in the vertical one). Each pixel has a 11 μm × 11 μm squared section. It should be remarked that the influence of the finite size of the pixels of the CCD device on the value of $\tilde{P}$ and $\tilde{\sigma}_p^2$ would be negligible provided that the number of pixels of the camera is large enough (say, $> 30 \times 30$) in the region where the beam intensity is significant.

In both cases five measurements have been performed for each configuration of the experimental setup. After averaging all these images, the Stokes parameters have been computed by using Eqs. (5.41)–(5.44). We finally obtain that the parameters $\tilde{P}$

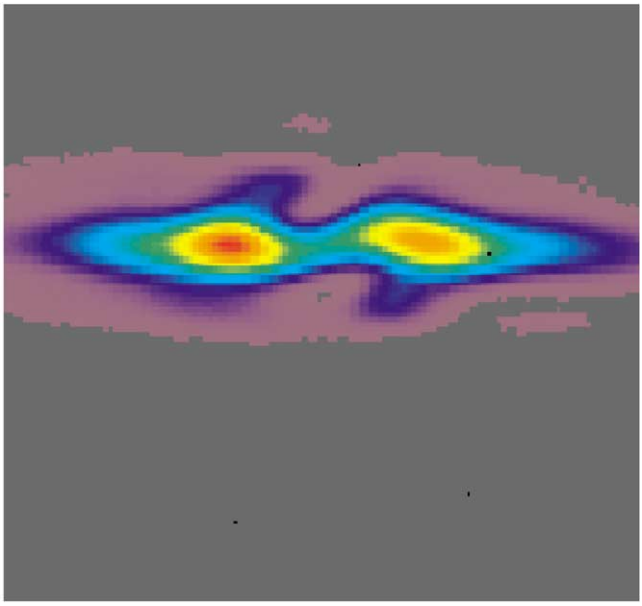

Fig. 20. Intensity distribution (pseudocoloured) at a transverse plane of the beam emitted by the laser diode LDM-135.

and $\tilde{\sigma}_p$ reach the following values:

Case i: $\tilde{P} = 1.005$; $\tilde{\sigma}_p = 9 \times 10^{-3}$.

These results confirm the specification given by the manufacturer ($P = 0.999$).

Case ii: $\tilde{P} = 0.93$; $\tilde{\sigma}_p = 0.003$.

Since $\tilde{P} < 1$ the field is not fully polarized. Furthermore, since $\tilde{\sigma}_p$ approaches zero, the beam could be considered as (nearly) uniformly polarized.

6. Quality improvement of partially polarized beams

High focusability (small beam width) along with low beam divergence at the far field are the required conditions in certain laser applications. It would then be useful to introduce a figure of merit that provides a joint description of the focussing and collimation capabilities of a laser beam. To this purpose, the so-called beam quality parameter, Q, has been defined for partially coherent scalar fields in terms of the second-order intensity moments [74,88]:

$$Q = \langle x^2 + y^2 \rangle \langle u^2 + v^2 \rangle - \langle xu + yv \rangle^2 = \langle r^2 \rangle \langle \eta^2 \rangle - \langle \mathbf{r} \cdot \boldsymbol{\eta} \rangle^2, \qquad (6.1)$$

where, again, for the sake of simplicity, it has been assumed that $\langle x \rangle = \langle y \rangle = \langle u \rangle = \langle v \rangle = 0$. In the above equation and in the remainder of this section we keep for the angle brackets the same notation introduced in Eq. (3.4). In particular, since $\langle xu + yv \rangle$ vanishes at the waist plane (minimum beam width), the parameter Q

reduces to the very simple expression

$$Q = \langle r^2 \rangle_w \langle \eta^2 \rangle, \tag{6.2}$$

where the subscript "w" refers to the waist. From this formula we see that the beam quality parameter contains simultaneous information of both the space and the spatial-frequency domains. In fact, Q characterizes the behavior of the beam at the near and at the far field. It should also be noted that the squared root of Q is identical, a factor $k = 2\pi/\lambda$ apart, to the so-called beam propagation factor, M^2, introduced by Siegman [94], namely

$$M^2 = kQ^{1/2}. \tag{6.3}$$

The parameter Q exhibits two outstanding and practical properties:

(i) It remains invariant under propagation through rotationally symmetric first-order optical systems (even for beams without such symmetry and with non-zero crossed moments, $\langle xy \rangle$, $\langle xv \rangle$, $\langle yu \rangle$ or $\langle uv \rangle$).

(ii) It has a lower limit (uncertainty relation)

$$Q \geqslant 1/k^2, \tag{6.4}$$

or, equivalently,

$$M^2 \geqslant 1, \tag{6.5}$$

where the equalities are only reached by a Gaussian beam (best quality). Note, in this sense, that the beam quality improves when Q takes lower values, and, conversely, the quality deteriorates when the numerical value of Q increases.

These features along with its simple measurement justify that the beam propagation factor M^2 has been accepted as the ISO beam quality standard [110]. In addition, a number of conditions and optical systems to improve this parameter have been reported in the literature in the last ten years [111–117].

A question, however, remains as to whether a relationship can be established between coherence and quality for arbitrary partially coherent beams. Unfortunately, the general answer is negative. Moreover, it is not difficult to find beams with different coherence characteristics having the same value of the quality parameter. Nevertheless, for certain fields a one-to-one correspondence exists between coherence and the value of Q: for example, for GSM scalar fields, defined by Eq. (5.35), the quality improves when the ratio $\delta = \sigma_\mu/\sigma_I$ increases (more specifically, Q is inversely proportional to δ^2).

It was pointed out at the beginning of this section that the parameter Q applies to scalar fields. Therefore, a generalization of the quality parameter for the vectorial case becomes necessary. This can be achieved by extending, in a natural way, the former definition of Q:

$$Q_G = \langle r^2 \rangle \langle \eta^2 \rangle - \langle \mathbf{r} \cdot \boldsymbol{\eta} \rangle^2, \tag{6.6}$$

where the subscript "G" stands for generalized definition, and the second-order moments of the global beam now include both components, namely

$$\langle r^2 \rangle = \frac{I_s}{I} \langle r^2 \rangle_s + \frac{I_p}{I} \langle r^2 \rangle_p, \tag{6.7}$$

$$\langle \eta^2 \rangle = \frac{I_s}{I} \langle \eta^2 \rangle_s + \frac{I_p}{I} \langle \eta^2 \rangle_p, \tag{6.8}$$

$$\langle \mathbf{r} \cdot \boldsymbol{\eta} \rangle = \frac{I_s}{I} \langle \mathbf{r} \cdot \boldsymbol{\eta} \rangle_s + \frac{I_p}{I} \langle \mathbf{r} \cdot \boldsymbol{\eta} \rangle_p. \tag{6.9}$$

In these equations

$$\langle \alpha\beta \rangle_i = \frac{1}{I_i} \frac{k^2}{4\pi^2} \int\int\int \alpha\beta \overline{E_i^*(\mathbf{r} + \mathbf{s}/2, z) E_i(\mathbf{r} - \mathbf{s}/2, z)} \exp(\mathrm{i}k\mathbf{s} \cdot \boldsymbol{\eta}) \, \mathrm{d}\mathbf{s} \, \mathrm{d}\mathbf{r} \, \mathrm{d}\boldsymbol{\eta},$$
$$i = s, p; \;\; \alpha, \beta = x, y, u, v \tag{6.10}$$

represent the second-order moments associated to the respective field components (the overbar symbolizes an ensemble average), $I_i = \int |E_i(\mathbf{r})|^2 \, \mathrm{d}\mathbf{r}$, $i = s, p$, denotes the intensity of the i-component, and $I = I_s + I_p$. The presence of the factors I_i/I, $i = s, p$, in the right-hand side of Eqs. (6.7)–(6.9) arises from the different normalization constants, I and I_i, of the moments associated to the global beam and to the field components, respectively.

The parameter Q_{G} can also be written in terms of the beam qualities, Q_s and Q_p, of the electric field components:

$$Q_{\mathrm{G}} = \left(\frac{I_s}{I}\right)^2 Q_s + \left(\frac{I_p}{I}\right)^2 Q_p + \left(\frac{I_s I_p}{I^2}\right) Q_{sp}, \tag{6.11}$$

where

$$Q_i = \langle r^2 \rangle_i \langle \eta^2 \rangle_i - \langle \mathbf{r} \cdot \boldsymbol{\eta} \rangle_i^2, \quad i = s, p \tag{6.12}$$

and

$$Q_{sp} = \langle r^2 \rangle \langle \eta^2 \rangle_p + \langle r^2 \rangle_p \langle \eta^2 \rangle_s - 2 \langle \mathbf{r} \cdot \boldsymbol{\eta} \rangle_s \langle \mathbf{r} \cdot \boldsymbol{\eta} \rangle_p. \tag{6.13}$$

As a simple example of application of this parameter let us again consider the beam emerging from an optically pumped Nd:YAG rod (see Section 5.4). It is easy to show that the value of Q_{G} at the output plane of the rod reads

$$Q_{\mathrm{G}} = \frac{1}{k^2}[1 + \beta + \ln(1 + \beta)]. \tag{6.14}$$

Consequently, the beam quality deteriorates when β grows. From the definition of the parameter β (see Eq. (5.23)), it can be concluded at once that, in order to obtain a better beam quality

(i) the pumping power should decrease, and/or
(ii) the radius of the rod should increase, and/or
(iii) the transverse beam size should reduce.

We thus see that the beam quality parameter could be of use in the design of this optical system. We do not proceed further into this analysis, which has been included for illustrative purposes only.

Once the generalized parameter Q_G has been introduced, attention will be focussed on the improvement of the beam quality. Because of the invariance property of parameter Q in the scalar case, no rotationally symmetric ABCD system could be employed to improve the quality of a partially coherent beam. However, such possibility exists when the vectorial nature of the light field is taken into account. In the next subsection, conditions will be given under which the quality parameter is optimized. We will focus on the use of a Mach–Zehnder-type (MZT) interferometric arrangement.

6.1. Beam quality changes after propagation through MZT systems

A MZT optical system resembles that of a typical Mach–Zehnder interferometer, but now with a polarizer in each arm (Fig. 21). To avoid interference between the emerging beams, the transmission axes of the linear polarizers has been chosen to be orthogonal. For the sake of simplicity, we deal here with rotationally symmetric beams and stigmatic non-polarizing first-order systems, whose ABCD matrices $\hat{\mathscr{S}}$ are composed of four submatrices proportional to the 2×2 identity matrix $\hat{I}$, i.e.,

$$\hat{\mathscr{S}} = \begin{pmatrix} A\hat{I} & B\hat{I} \\ C\hat{I} & D\hat{I} \end{pmatrix}, \tag{6.15}$$

where A, B, C and D are constants. For this kind of systems Q_G remains invariant. Also note that the stigmatic systems allow to generate, in an easy way, non-uniformly polarized beams. A simple example is provided by the polarization diagram sketched in Fig. 22: the incident beam is Gaussian, linearly polarized at 45° with respect to the transmission axes of the polarizers, its Rayleigh length is $z_R = 10$ cm and its waist is placed 10 cm away from the input plane of the interferometer. The ABCD systems are free-propagation regions whose lengths are $L_1 = 10$ cm and $L_2 = 20$ cm. We see that, after recombination, the output beam is no longer linearly polarized and, in addition, its polarization state is not uniform across the beam

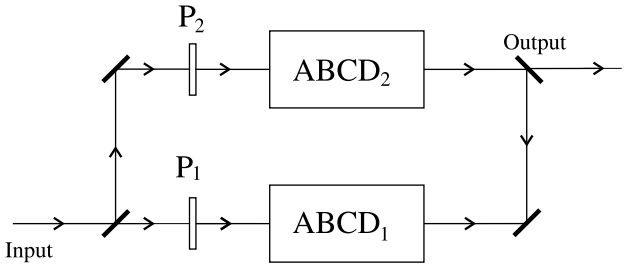

Fig. 21. Schematic of a general MZT optical system.

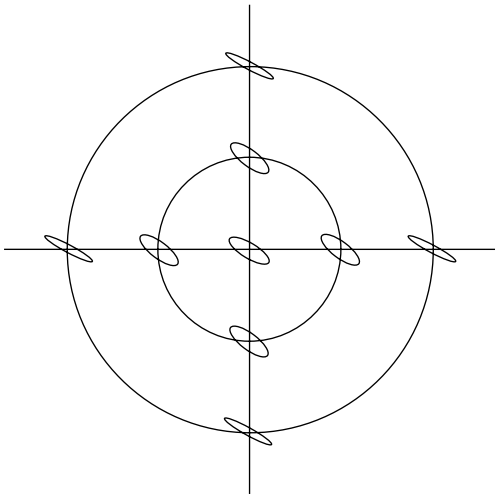

Fig. 22. Schematic of the spatial distribution of the polarization state at the output plane of a certain MZT system (for details, see text).

section (the ellipticity of the polarization ellipses depends on the radial distance to the beam center).

It follows from Fig. 21 that the second-order moments associated to each beam component propagate according to the well-known ABCD law

$$\langle r^2 \rangle_m^{\mathrm{o}} = A_m^2 \langle r^2 \rangle_m^{\mathrm{i}} + 2A_m B_m \langle \mathbf{r} \cdot \boldsymbol{\eta} \rangle_m^{\mathrm{i}} + B_m^2 \langle \eta^2 \rangle_m^{\mathrm{i}}, \tag{6.16}$$

$$\langle \mathbf{r} \cdot \boldsymbol{\eta} \rangle_m^{\mathrm{o}} = A_m C_m \langle r^2 \rangle_m^{\mathrm{i}} + (A_m D_m + B_m C_m) \langle \mathbf{r} \cdot \boldsymbol{\eta} \rangle_m^{\mathrm{i}} + B_m D_m \langle \eta^2 \rangle_m^{\mathrm{i}}, \tag{6.17}$$

$$\langle \eta^2 \rangle_m^{\mathrm{o}} = C_m^2 \langle r^2 \rangle_m^{\mathrm{i}} + 2C_m D_m \langle \mathbf{r} \cdot \boldsymbol{\eta} \rangle_m^{\mathrm{i}} + D_m^2 \langle \eta^2 \rangle_m^{\mathrm{i}}, \quad m = s, p, \tag{6.18}$$

where the superscripts "i" and "o" denote the input and output planes of the optical arrangement. Accordingly, the intensity moment of the output global beam can be inferred in terms of their values at the input plane from direct substitution of Eqs. (6.16)–(6.18) into Eqs. (6.7)–(6.9).

For convenience, we will analyze three classes of MZT devices in which the first-order optical systems are: (a) free propagation sections; (b) magnifiers; (c) thin lenses. As it will be apparent in Section 6.2, such systems summarizes the procedure we have to follow to optimize the beam quality parameter.

(a) *Free propagation*

In this case, the field freely propagates along the two arms of the MZT system, but the respective propagation distances, L_1 and L_2, are different. Consequently, the elements of the ABCD matrices are

$$A_1 = 1, \qquad B_1 = L_1, \quad C_1 = 0, \quad D_1 = 1, \tag{6.19}$$

$$A_2 = 1, \qquad B_2 = L_2, \quad C_2 = 0, \quad D_2 = 1. \tag{6.20}$$

It can be shown for this kind of systems [118] that the necessary and sufficient condition for improving the quality parameter of the emerging beam reduces to

$$|L_2 - L_1| < 2|H_s - H_p|, \tag{6.21}$$

provided that

$$\mathrm{sign}(L_2 - L_1) = \mathrm{sign}(H_s - H_p), \tag{6.22}$$

where

$$H_j \equiv \frac{\langle \mathbf{r} \cdot \boldsymbol{\eta} \rangle_j}{\langle \eta^2 \rangle_j}, \quad j = s, p \tag{6.23}$$

and the averages are evaluated at the input plane. Furthermore, this improvement is optimized when the difference $L_2 - L_1$ is identical to the distance L between the waist planes associated to each component of the input beam (see Fig. 23). In this sense, note that H_s and H_p are the distances between the input plane and the waist planes associated to the s and p components, respectively. The optimum quality improvement then becomes

$$(\Delta Q_{\mathrm{G}})_{\mathrm{opt}} \equiv Q_{\mathrm{G}}^{\mathrm{o}} - Q_{\mathrm{G}}^{\mathrm{i}} = -\frac{I_s I_p}{I^2} \langle \eta^2 \rangle_s \langle \eta^2 \rangle_p L^2. \tag{6.24}$$

Accordingly, it can be concluded that the best quality is attained when the difference between the free-propagation lengths of the MZT interferometer exactly compensates for the distance between the waists of the components of the input beam. In particular, when the distances are much longer than the Rayleigh length of the beam, the ratio H_j, $j = s, p$, approaches the radius of curvature of the wavefront associated to each component at the far field.

(b) *Magnifiers*

As is well known, a magnifier behaves as a first-order optical system that increases the minimum beam size by a factor m (and the beam divergence is multiplied by a factor m^{-1}). The combined effect is a change of the Rayleigh length of the beam. Here we consider MZT systems whose ABCD components are magnifiers. The

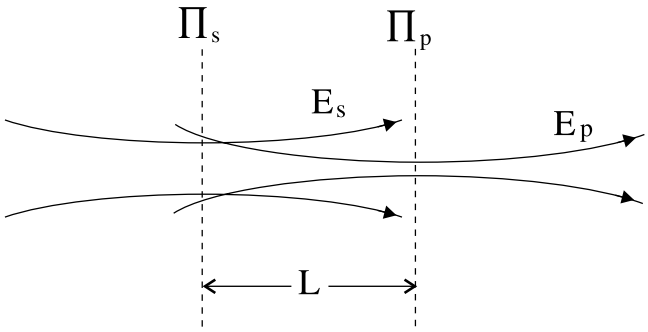

Fig. 23. Schematic of the relative position of the waists associated to the electric field components E_s and E_p. Π_s and Π_p indicate the respective waist planes (for details, see text).

corresponding ABCD matrices are

$$A_1 = m_1, \qquad B_1 = 0, \qquad C_1 = 0, \qquad D_1 = m_1^{-1}, \tag{6.25}$$

$$A_2 = m_2, \qquad B_2 = 0, \qquad C_2 = 0, \qquad D_2 = m_2^{-1}. \tag{6.26}$$

Let us now define the parameters

$$m \equiv m_1 m_2^{-1} \tag{6.27}$$

and

$$a \equiv \frac{\langle r^2 \rangle_p \langle \eta^2 \rangle_s}{\langle r^2 \rangle_s \langle \eta^2 \rangle_p}. \tag{6.28}$$

In terms of these parameters, it can be shown [118] that the beam quality of the output field may be improved by choosing two magnifiers that satisfy

$$\min(1, a) < m^2 < \max(1, a). \tag{6.29}$$

To get deeper insight into the physical meaning of this condition, let us consider, for simplicity, that the waists of both field components are placed at the input plane of the MZT system. It then follows that the quality parameter Q_G will be optimized provided

$$m^2 = \frac{z_{R_p}}{z_{R_s}}, \tag{6.30}$$

where z_{R_p} and z_{R_s} represent the Rayleigh length of the s and p components, respectively. In such a case we finally have

$$(\Delta Q_G)_{opt} = -\frac{I_s I_p}{I^2} \langle \eta^2 \rangle_s \langle \eta^2 \rangle_p (z_{R_s} - z_{R_p})^2. \tag{6.31}$$

From this expression it is now apparent that, to optimize Q_G, the MZT arrangement should compensate for the difference in Rayleigh lengths associated to each incident beam component.

(c) *Thin lenses*

Let us now handle MZT systems with a thin lens in each arm (Fig. 24). Such configuration is equivalent, to our purposes, to a lenslike birefringent medium, which can either be considered as a thin lens made of an anisotropic homogeneous material or as a plane-parallel plate made of a uniaxial medium whose inhomogeneous principal indices show a transversal quadratic dependence on the radial distance to the propagation axis (Fig. 25). Applications of such components include laser cavities designed to get predetermined profiles and spatial filtering [17–19], to mention only two. Also note that these optical devices maintain the total beam power (they may be regarded as pure phase transmittances).

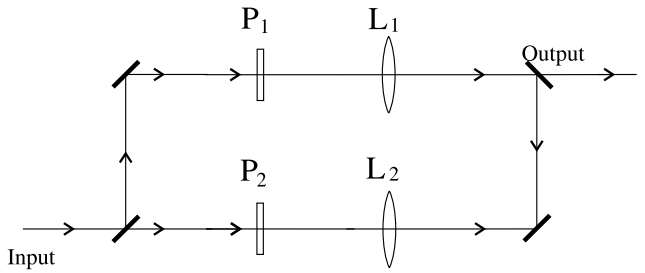

Fig. 24. Schematic of an MZT optical system with a thin lens in each arm. The focal lengths of the converging thin lenses L_1 and L_2 are f_1 and f_2, respectively. P_1 and P_2 are again orthogonally orientated linear polarizers.

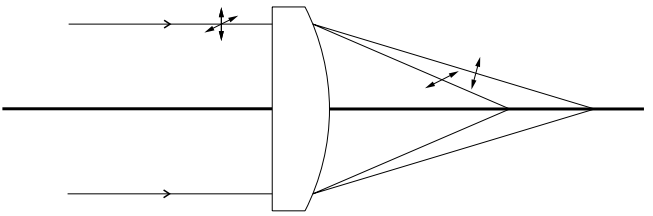

Fig. 25. Planoconvex birefringent lens: the arrows indicate that the electric field components of the incident beam are focussed on different planes. The optic axis is parallel to the planar face of the lens.

The elements of the ABCD matrices that characterizes such systems are

$$A_1 = 1, \qquad B_1 = 0, \qquad C_1 = -\frac{1}{f_1}, \qquad D_1 = 1, \tag{6.32}$$

$$A_2 = 1, \qquad B_2 = 0, \qquad C_2 = -\frac{1}{f_2}, \qquad D_2 = 1. \tag{6.33}$$

If we use this kind of systems to improve Q_G, it can be shown [119] that the beam quality always degrades for uniformly totally polarized beams as well as for non-polarized fields. However, the quality parameter may be improved whenever

$$\left|\frac{1}{f_2} - \frac{1}{f_1}\right| < 2\left|\frac{1}{R_s} - \frac{1}{R_p}\right|, \tag{6.34}$$

where R_s and R_p denote the overall curvature radius of the wavefronts associated to the field components, i.e.,

$$R_j = \frac{\langle r^2 \rangle_j}{\langle \mathbf{r} \cdot \boldsymbol{\eta} \rangle_j}, \quad j = s, p \tag{6.35}$$

and the averages are computed at the input plane. In the particular case in which we handle an anisotropic planoconvex lens, the above condition becomes

$$\left|\frac{n_o - n_e}{R_L}\right| < 2\left|\frac{1}{R_s} - \frac{1}{R_p}\right|, \tag{6.36}$$

where n_e and n_o denote the extraordinary and the ordinary refractive index of the medium, respectively, and R_L represents the curvature radius of the convex face of the birefringent lens.

In addition, the optimum value of the beam quality is reached when

$$\left|\frac{1}{f_2}-\frac{1}{f_1}\right| = \frac{1}{R_s}-\frac{1}{R_p} \tag{6.37}$$

and the optimum quality improvement reads

$$(\Delta Q)_{\text{opt}} = -\frac{I_s I_p}{I^2}\langle r^2\rangle_s\langle r^2\rangle_p\left(\frac{1}{R_s}-\frac{1}{R_p}\right)^2. \tag{6.38}$$

We then conclude that, to optimize the quality parameter, this MZT system should exactly compensate for the difference in the curvature radii of the wavefronts associated to each incident beam component.

6.2. Beam quality optimization: general condition

In the previous section some conditions were derived to optimize the generalized quality parameter of a beam by acting on its orthogonal components. In all the cases, the optical system should compensate for the differences in several magnitudes (expressed in terms of second-order moments) associated to each incident field component. Here we will give the general condition to be fulfilled by the intensity moments in order to optimize the quality of the global beam.

Since Q_G is invariant under rotation around the mean propagation direction ($\langle u\rangle = \langle v\rangle = 0$), for convenience we refer our analysis to the reference coordinate system with respect to which $I_s = I_p$. In terms of this new coordinate system, the beam quality parameter reduces to

$$Q_G = \tfrac{1}{4}(Q_s + Q_p + Q_{sp}), \tag{6.39}$$

where Q_s, Q_p and Q_{sp} were introduced in Eqs. (6.12) and (6.13). Let us now assume, without loss of generality, that the s-component reaches its waist at the plane where the moments are evaluated. This implies

$$\langle \mathbf{r}\cdot\boldsymbol{\eta}\rangle_s = 0. \tag{6.40}$$

The parameter Q_G then becomes

$$Q_G = \tfrac{1}{4}(Q_s + Q_p + \langle r^2\rangle_s\langle \eta^2\rangle_p + \langle r^2\rangle_p\langle \eta^2\rangle_s). \tag{6.41}$$

Since Q_s, Q_p, $\langle r^2\rangle_s\langle \eta^2\rangle_p$ and $\langle r^2\rangle_p\langle \eta^2\rangle_s$ are positive quantities, it can be shown that

$$Q_G^2 \geqslant Q_s Q_p. \tag{6.42}$$

In particular, the equality is fulfilled provided that the following relations hold:

$$\langle r^2 \rangle_s = \langle r^2 \rangle_p, \tag{6.43}$$

$$\langle \eta^2 \rangle_s = \langle \eta^2 \rangle_p, \tag{6.44}$$

$$\langle \mathbf{r} \cdot \boldsymbol{\eta} \rangle_s = \langle \mathbf{r} \cdot \boldsymbol{\eta} \rangle_p = 0. \tag{6.45}$$

In other words, the beam quality parameter will reach its minimum value (best quality) when the second-order moments associated to each transverse field component are identical (remember that the coordinate system should be chosen to make I_s equal to I_p). We thus see that the optimization conditions we obtained for the three configurations analyzed in Section 6.1 are closely related with Eqs. (6.43)–(6.45). Moreover, this suggests that a general scheme to improve the quality parameter Q_G of a partially polarized beam might consist of a MZT arrangement with free propagation regions to compensate for the different waist positions of their components, followed by a second MZT system that contains magnifiers to compensate for the corresponding Rayleigh lengths.

7. Non-paraxial electromagnetic vector beams

Throughout the present paper, the treatment of the polarization properties of electromagnetic beams has been restricted to the paraxial regime and the subsequent quasi-transversality approximation. This is suited for nearly plane waves whose propagation directions have a small range about a given direction, as occurs for typical laser beams. In addition, descriptions of light fields based on the solution of the scalar Helmholtz equation (associated to each Cartesian beam component) in the paraxial limit imply to use linearly polarized beams or, equivalently, to consider a single component of the field. Although many different beams and optical systems can be handled by means of these simple models, the above approaches involve, however, several weaknesses: note, for example, that the typical linearly polarized Gaussian beam we have studied along this work is not an exact solution of the Maxwell equations. Furthermore, no word has still been said about the polarization behavior of a vector field in the non-paraxial case. It seems then appropriate to devote some effort at the end of this paper to discuss this kind of problems, which are receiving increasing attention in the literature [40–51].

Starting from the Maxwell equations, vectorial formulations are being developed in the past few years. They include localized Bessel–Gauss solutions [41] as well as optical beams generated by planar sources with different states of coherence [45]. Here our attention will be focussed on the vectorial structure of electromagnetic beams in the non-paraxial regime. Our procedure employs a representation of the general solution of the Maxwell equations in terms of the angular plane-wave spectrum of the electromagnetic field. Alternative treatments of the non-paraxial case on the basis of the Hertz vectors or by using the complex source-point model can be found in Refs. [42,44,46,49]. Furthermore, the geometry of non-paraxial

complex vector waves has been explored by regarding them as a field of polarization ellipses [40,47].

7.1. Plane-wave spectrum solution of the electromagnetic field

For the sake of simplicity, we consider time-harmonic electric and magnetic fields, **E** and **H**, respectively, fulfilling the Maxwell equations in a homogeneous isotropic medium

$$\nabla \times \mathbf{H} + \mathrm{i}k\mathbf{E} = 0, \tag{7.1}$$

$$\nabla \times \mathbf{E} - \mathrm{i}k\mathbf{H} = 0, \tag{7.2}$$

$$\nabla \cdot \mathbf{E} = \nabla \cdot \mathbf{H} = 0. \tag{7.3}$$

Both fields **E** and **H** can be expressed in terms of their respective angular plane-wave spectrum (with respect to an arbitrary, but fixed, Cartesian coordinate system) in the form

$$\mathbf{E}(x, y, z) = \int\int \tilde{\mathbf{E}}(u, v, z)\exp[\mathrm{i}k(xu + yv)]\,\mathrm{d}u\,\mathrm{d}v, \tag{7.4}$$

$$\mathbf{H}(x, y, z) = \int\int \tilde{\mathbf{H}}(u, v, z)\exp[\mathrm{i}k(xu + yv)]\,\mathrm{d}u\,\mathrm{d}v, \tag{7.5}$$

where $\tilde{\mathbf{E}}$ and $\tilde{\mathbf{H}}$ represent the spatial Fourier transforms of **E** and **H**, respectively. Although x, y and z are, in principle, equivalent directions, we choose here the z-axis as the direction of propagation of the beam.

For convenience, let us introduce planar polar coordinates (ϕ, ρ) defined by the relations

$$u = \rho\cos\phi, \tag{7.6}$$

$$v = \rho\sin\phi. \tag{7.7}$$

Under the assumption of propagation distances z long enough to neglect the contribution of the evanescent waves, the variable ρ takes values only in the interval $[0, 1]$. Taking this into account, from the substitution of Eqs. (7.4) and (7.5) into Eqs. (7.1)–(7.3), we obtain for the angular spectrum the solution

$$\tilde{\mathbf{E}}(\rho, \phi, z) = \tilde{\mathbf{E}}_0(\rho, \phi)\exp[\mathrm{i}kz(1 - \rho^2)^{1/2}], \tag{7.8}$$

$$\tilde{\mathbf{H}}(\rho, \phi, z) = \mathbf{s}(\rho, \phi) \times \tilde{\mathbf{E}}_0(\rho, \phi)\exp[\mathrm{i}kz(1 - \rho^2)^{1/2}], \tag{7.9}$$

with

$$\tilde{\mathbf{E}}_0(\rho, \phi) \cdot \mathbf{s}(\rho, \phi) = 0, \tag{7.10}$$

where

$$\mathbf{s}(\rho, \phi) = [\rho\cos\phi, \rho\sin\phi, (1 - \rho^2)^{1/2}] \tag{7.11}$$

is a unit vector in the direction of the plane-wave components. Let us now write $\tilde{\mathbf{E}}_0$ in the form [50]

$$\tilde{\mathbf{E}}_0(\rho,\phi) = a(\rho,\phi)\mathbf{e}_1(\rho,\phi) + b(\rho,\phi)\mathbf{e}_2(\rho,\phi), \tag{7.12}$$

where

$$a(\rho,\phi) = \tilde{\mathbf{E}}_0 \cdot \mathbf{e}_1, \tag{7.13}$$

$$b(\rho,\phi) = \tilde{\mathbf{E}}_0 \cdot \mathbf{e}_2, \tag{7.14}$$

are integrable functions, and

$$\mathbf{e}_1 = (\sin\phi, -\cos\phi, 0), \tag{7.15}$$

$$\mathbf{e}_2 = [(1-\rho^2)^{1/2}\cos\phi, (1-\rho^2)^{1/2}\sin\phi, -\rho]. \tag{7.16}$$

It can be shown at once that $\mathbf{s}$, $\mathbf{e}_1$ and $\mathbf{e}_2$ form a triad of a mutually orthogonal right-handed system of unit vectors. The electric field solution of the Maxwell equations can then be written as the sum of two terms, $\mathbf{E}_{\mathrm{TE}}(\mathbf{r})$ and $\mathbf{E}_{\mathrm{TM}}(\mathbf{r})$, given by

$$\mathbf{E}_{\mathrm{TE}}(\mathbf{r}) = \int_0^1 \int_0^{2\pi} a(\rho,\phi)\mathbf{e}_1 \exp(\mathrm{i}k\mathbf{r}\cdot\mathbf{s})\rho \,\mathrm{d}\rho \,\mathrm{d}\phi, \tag{7.17}$$

$$\mathbf{E}_{\mathrm{TM}}(\mathbf{r}) = \int_0^1 \int_0^{2\pi} b(\rho,\phi)\mathbf{e}_2 \exp(\mathrm{i}k\mathbf{r}\cdot\mathbf{s})\rho \,\mathrm{d}\rho \,\mathrm{d}\phi, \tag{7.18}$$

where $\mathbf{r} = (x, y, z)$. Furthermore, the following properties apply:

(i) $\mathbf{E}_{\mathrm{TE}}$ is a field orthogonal to the z direction.
(ii) $\mathbf{H}_{\mathrm{TM}}$, associated to $\mathbf{E}_{\mathrm{TE}}$, is also orthogonal to the z-axis.
(iii) $\mathbf{E}_{\mathrm{TE}}$ and $\mathbf{E}_{\mathrm{TM}}$ are orthogonal to each other at the far field.

In addition, the typical electromagnetic plane wave traveling in the z direction can be inferred from Eqs. (7.17) and (7.18) by choosing either

$$a(\rho,\phi) = \frac{a_0}{\rho}\delta(\phi)\delta(\rho), \tag{7.19}$$

$$b(\rho,\phi) = 0, \tag{7.20}$$

for the y-polarized case, or

$$a(\rho,\phi) = \frac{a_0}{\rho}\delta\left(\phi - \frac{\pi}{2}\right)\delta(\rho), \tag{7.21}$$

$$b(\rho,\phi) = 0, \tag{7.22}$$

for the x-polarized case, where a_0 is a constant and the symbol δ denotes, as usual, the Dirac delta function.

It should be stressed that the above explicit solutions for the electric and the magnetic field vectors are valid in the non-paraxial case. The common paraxial

approach would follow from the substitutions

$$\exp[ikz(1-\rho^2)^{1/2}] \cong \exp(ikz)\exp\left(-ikz\frac{\rho^2}{2}\right), \tag{7.23}$$

$$\mathbf{e}_2 = (\cos\phi, \sin\phi, 0), \tag{7.24}$$

in the corresponding expressions (see also Eq. (2.14)).

We next apply the solutions (7.17) and (7.18) to certain examples of interest.

7.2. Closest solution to a vector field

Let us suppose that we try to model a certain electromagnetic field at the plane, say, $z = 0$ by means of an easy-to-use vector function $\mathbf{f}(x, y)$. It might happen that no exact solution exists of the Maxwell equations such that the electric vector $\mathbf{E}$ equals $\mathbf{f}(x, y)$ at $z = 0$. In such a case, we could define the *closest* solution to $\mathbf{f}$ as the *exact* solution of the Maxwell equations that is best fitted (in an algebraic sense) to function $\mathbf{f}$. To understand what this means let us first express $\mathbf{f}$ in terms of its plane-wave spectrum, namely

$$\mathbf{f}(x, y) = \int_0^1 \int_0^{2\pi} \tilde{\mathbf{f}}(\rho, \phi) \exp[ik(x\rho\cos\phi + y\rho\sin\phi)]\rho \, d\rho \, d\phi, \tag{7.25}$$

where the evanescent waves have been neglected. The projection of vector $\tilde{\mathbf{f}}$ onto the (two-dimensional) subspace generated by $\mathbf{e}_1$ and $\mathbf{e}_2$ is given by $(\tilde{\mathbf{f}} \cdot \mathbf{e}_1)\mathbf{e}_1 + (\tilde{\mathbf{f}} \cdot \mathbf{e}_2)\mathbf{e}_2$, which is, from an algebraic point of view, the vector function closest to $\tilde{\mathbf{f}}$ that fulfills Eq. (7.12). Accordingly, the electric field vector $\mathbf{E}_f$, solution of the Maxwell equations, that is closest to $\mathbf{f}$ is given by [50]

$$\begin{aligned}\mathbf{E}_f(\mathbf{r}) = &\int_0^1 \int_0^{2\pi} (\tilde{\mathbf{f}} \cdot \mathbf{e}_1)\mathbf{e}_1 \exp(ik\mathbf{r} \cdot \mathbf{s})\rho \, d\rho \, d\phi \\ &+ \int_0^1 \int_0^{2\pi} (\tilde{\mathbf{f}} \cdot \mathbf{e}_2)\mathbf{e}_2 \exp(ik\mathbf{r} \cdot \mathbf{s})\rho \, d\rho \, d\phi,\end{aligned} \tag{7.26}$$

where we have used Eqs. (7.17) and (7.18). It is clear that the first term of the above equation would represent the transverse electric field $\mathbf{E}_{\mathrm{TE}}$ closest to $\mathbf{f}$.

To illustrate this concept let us consider a linearly polarized Gaussian field that propagates along the z-axis. Since this kind of beam does not fulfill the condition $\nabla \cdot \mathbf{E} = 0$ (see Eq. (7.3)), it cannot be accepted as an exact solution of the complete Maxwell equations. To get the associated closest solution, let us write the Gaussian field at the plane $z = 0$ in the form

$$\mathbf{f}_{\mathrm{G}} = \mathbf{i}C \int_0^1 \int_0^{2\pi} \exp\left[-\left(\frac{\rho^2}{D^2}\right)\right] \exp[ik(x\rho\cos\phi + y\rho\sin\phi)]\rho \, d\rho \, d\phi, \tag{7.27}$$

where $\mathbf{i}$ denotes a unit vector in the x direction that defines the linear polarization of the beam, D is a constant proportional to the beam divergence at the far field, and C is a normalization constant. According to Eq. (7.26), the vector field $\mathbf{E}_{\mathrm{G}}$ closest

to $\mathbf{f}_G$ reads

$$\mathbf{E}_G = (\mathbf{E}_{TE})_G + (\mathbf{E}_{TM})_G, \tag{7.28}$$

where

$$(\mathbf{E}_{TE})_G = C \int_0^1 \int_0^{2\pi} \sin\phi \exp\left[-\left(\frac{\rho^2}{D^2}\right)\right] \exp(ik\mathbf{r}\cdot\mathbf{s})\mathbf{e}_1 \rho \, d\rho \, d\phi, \tag{7.29}$$

$$(\mathbf{E}_{TM})_G = C \int_0^1 \int_0^{2\pi} \cos\phi (1-\rho^2)^{1/2} \exp\left[-\left(\frac{\rho^2}{D^2}\right)\right] \exp(ik\mathbf{r}\cdot\mathbf{s})\mathbf{e}_2 \rho \, d\rho \, d\phi. \tag{7.30}$$

We see that, unlike the Gaussian beam, its associated closest solution is not a uniformly polarized field. In addition, the closest field $\mathbf{E}_G$ is identical to the Gaussian vectorial wave proposed in Ref. [42].

Figs. 26 and 27 illustrate the spatial structure of $\mathbf{E}_G$. To enhance the vectorial effects, we plot the curves for a Gaussian beam whose transverse size at the waist plane $z = 0$ is equal to one wavelength. This is equivalent to choosing the value of $D = (2\pi)^{-1}$. It should be pointed out that, in contrast to the linearly polarized Gaussian case, the transverse component of its closest field, $(\mathbf{E}_{TE})_G$, shows an important contribution of its (four-lobe) y-component. Furthermore, the corresponding intensity profile $|\mathbf{E}_{TE}|^2$ is no longer Gaussian and shows a non-rotationally symmetric shape, which arises from the linear polarization along the x-axis.

Also note that the global field $\mathbf{E}_G$ exhibits a two-lobe longitudinal component $(\mathbf{E}_{TM})_z$ along the z-axis, which would be negligible in the paraxial limit (quasi-transversality approximation). In the present (non-paraxial) case, the longitudinal component is one order of magnitude lower than the transverse x-component.

Let us finally remark that the results discussed in this section should be considered as preliminary developments. At present, a complete overall vector characterization of this type of non-uniformly polarized non-paraxial fields is still an open problem, which deserves further study in the future.

8. Conclusions

In the paraxial regime, a global description of partially polarized partially coherent beams has been established. A family of global parameters (including new degrees of polarization) have been introduced. Such parameters have been shown to represent easy-to-measure physically meaningful quantities, which provide information about both the spatial structure and the uniformity of the polarization distribution of the beam profile. The main advantage of this characterization procedure arises from the simple propagation laws of the parameters along first-order optical systems and through polarization-altering devices represented by Mueller matrices.

Thus, once the global parameters have been measured at some input plane, their values can be easily computed at the output of the optical system. This may be used

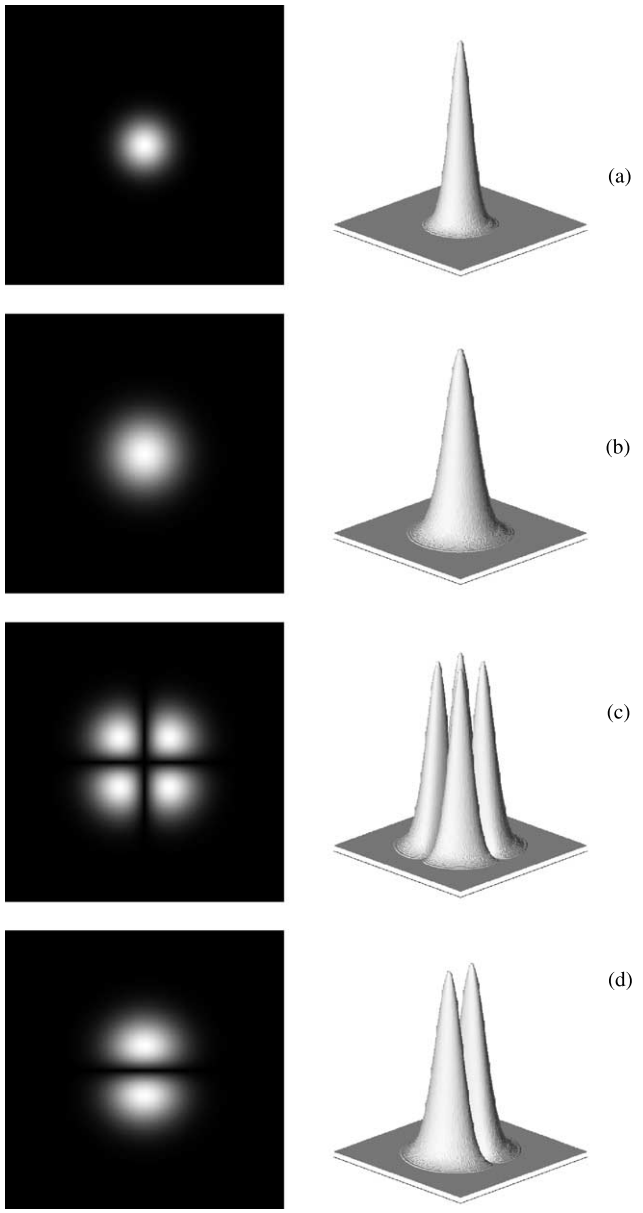

Fig. 26. Spatial structure of the closest field $\mathbf{E}_G$ associated to a linearly polarized Gaussian beam: (a) intensity profile; (b) modulus of the global x-component $|(E_x)_{TE} + (E_x)_{TM}|$; (c) modulus of the global y-component $|(E_y)_{TE} + (E_y)_{TM}|$; (d) modulus of the longitudinal z-component $|(E_{TM})_z|$ (the transverse term $\mathbf{E}_{TE}$ has no component along z). For comparative purposes, note that $|(E_G)_x|_{max}/|(E_G)_y|_{max} = 211.9$ and $|(E_G)_x|_{max}/|(E_G)_z|_{max} = 14.7$, where the subscript max refers to the respective maximum values.

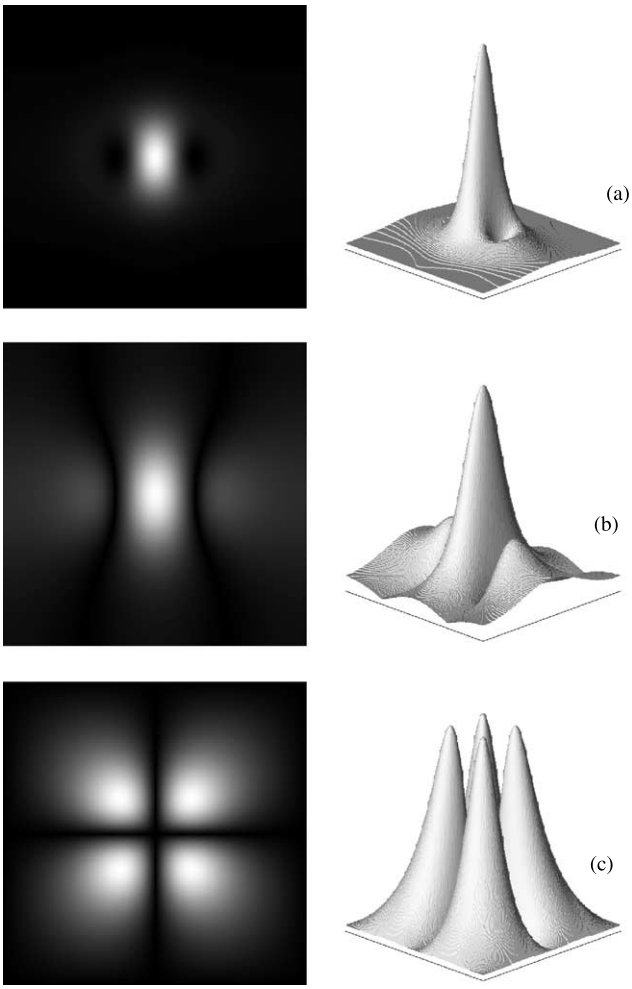

Fig. 27. Spatial structure of the transverse term $(\mathbf{E}_{TE})_G$ that is associated to a linearly polarized Gaussian beam: (a) intensity profile I_{TE}; (b) modulus of the x-component $|E_x|$ of the transverse term; (c) modulus of the y-component $|E_y|$ of the transverse term (the z component is zero). At each point $I_{TE} = |E_x|^2 + |E_y|^2$, as expected. In the present case $|E_x|_{max}/|E_y|_{max} = 3.23$.

in the design of optical arrangements, polarization shaping and beam quality improvement, to mention some applications.

A number of explicit or underlying restrictions have been assumed throughout the paper. Most of them are related to open questions whose analytical treatment deserves further attention in the future: apart from the non-paraxial case, we could mention, for example, the use of dispersive optical elements crossed by ultrashort laser pulses, the appearance of hard-edge diffracting apertures and the utilization of non-linear optical effects and devices.

Finally, we want to emphasize that the content and the conclusion of the present paper should not be considered as an ultimate recommendation and preference for our formalism to the detriment of alternative representations. In fact, to date, none of the existing characterization methods could be completely adopted without the appearance of theoretical or experimental limitations. Furthermore, it is not clear that a single representation procedure could be employed in all situations. And, in addition, we have seen that much more work is still needed. Accordingly, we feel that it would certainly be premature to establish an absolute choice. In any case, we hope this paper encourages further research in this field.

Acknowledgements

The research work leading to this paper was supported by the Ministerio de Educación y Cultura of Spain, Projects PB97-0295 and BFM 2001–1356, within the framework of EUREKA projects EU-1269 and EU-2359. The curves plotted in Figs. 26 and 27 were numerically computed by Drs. S. Bosch and A. Carnicer. We would also like to thank Prof. H. Weber, Mr. A. Vazquez and Mr. G. Mann from the Optisches Institut at the Technische Universität in Berlin for their continuous interest and support all along the experimental work described in Section 5.4. We are also grateful to Dr. J. Serna for helpful discussions and for his assistance in the preparation of this manuscript. One of the authors (G.P.) wishes to thank Prof. F. Gori, Dr. M. Santarsiero and Dr. R. Borghi for helpful discussions concerning PGSM sources.

References

[1] L. Mandel, E. Wolf, Optical Coherence and Quantum Optics, Cambridge University Press, Cambridge, 1995.
[2] A. Aspect, J. Dalibard, G. Roger, Experimental test of Bell's inequalities using time-varying analyzers, Physical Review Letters 49 (25) (1982) 1804–1807.
[3] S.F. Mason, Molecular Optical Activity and the Chiral Discrimination, Cambridge University Press, Cambridge, 1982.
[4] M.V. Berry, Quantal phase factors accompanying adiabatic changes, Proceedings of the Royal Society of London A 392 (1984) 45–57.
[5] H. Schmitzer, Nonlinearity of Pancharatnam's Topological phase, S. Klein, W. Dultz, Physical Review Letters 71 (10) (1993) 1530–1533.
[6] W.A. Shurcliff, Polarized Light, Harvard University Press, Cambridge, MA, 1962.
[7] W.G. Egan, Photometry and Polarization in Remote Sensing, Elsevier, New York, 1985.
[8] G.P. Konnen, Polarized Light in Nature, Cambridge University, Cambridge, 1985.
[9] R.M.A. Azzam, N.M. Bashara, Ellipsometry and Polarized Light, North-Holland, Amsterdam, 1987.
[10] K.L. Coulson, Polarization and Intensity Light in the Atmosphere, A. Deepak, Hampton, VA, 1988.
[11] D.S. Kliger, J.W. Lewis, C.E. Randall, Polarized Light in Optics and Spectroscopy, Academic Press, Boston, 1990.
[12] E. Collett, Polarized Light, Marcel Dekker Inc, New York, 1992.

[13] W. Boerner, H. Motts (Eds.), Radar Polarimetry, Proceedings SPIE, 1747, The International Society for Optical Engineering, Bellingham, 1992.
[14] M. Bass (Ed.), Handbook on Optics, Vols. I and II, McGraw-Hill, New York, 1994.
[15] C. Brosseau, Fundamentals of Polarized Light, Wiley, New York, 1998.
[16] D. Fink, Polarization effects of axicons, Applied Optics 18 (5) (1979) 581–582.
[17] B.J. Feldman, S.J. Gitomer, Anular lens soft aperture for high power laser systems, Applied Optics 15 (6) (1976) 1379–1380.
[18] G. Giuliani, Y.K. Park, R.L. Byer, Radial birefringent element and its applications to laser resonator design, Optical Letters 5 (11) (1980) 491–493.
[19] J.M. Eggleston, G. Giuliani, R.L. Byer, Radial intensity filters using radial birefringent elements, Journal of the Optical Society of America 71 (10) (1981) 1264–1272.
[20] S.C. Tidwell, D.H. Ford, W.D. Kimura, Generating radially polarized beams interferometrically, Applied Optics 29 (15) (1990) 2334–2339.
[21] T. Erdogan, D.G. Hall, Circularly symmetric distributed feedback semiconductor laser: an analysis, Journal of Applied Physics 68 (4) (1990) 1435–1444.
[22] T. Erdogan, O. King, G.W. Wicks, D.G. Hall, E. Anderson, M.J. Rooks, Circularly symmetric operation of a concentric-circle-grating surface emitting AlGaAs/GaAs quantum well semiconductor laser, Applied Physics Letters 60 (16) (1992) 1921–1923.
[23] S.C. Tidwell, G.H. Kim, W.D. Kimura, Efficient radially polarized laser beam generation with a double interferometer, Applied Optics 32 (27) (1993) 5222–5227.
[24] P.L. Greene, D.G. Hall, Diffraction characteristics of the azimuthal Bessel–Gauss beam, Journal of the Optical Society of America A 13 (9) (1996) 962–966.
[25] S. Sato, K. Takahashi, B. Mehmetli, Polarization effects of a high-power CO/sub2/laser beam on aluminum alloy weldability, Journal of Applied Physics 79 (12) (1996) 8917–8919.
[26] B. Lü, Y. Ye, Z. Sui, B. Cai, Analysis of a radially varying transmission system used for spatial beam shaping, Optik 101 (3) (1996) 97–100.
[27] I. Freund, Polarization flowers, Optics Communications 199 (1–4) (2001) 47–63.
[28] R.A. Chipman, Polarimetry, Hanbook on Optics, Vol. II, McGraw-Hill, New York, 1994 (Chapter 22).
[29] D.F.V. James, Change of polarization of light beams on propagation in free space, Journal of the Optical Society of America A 11 (5) (1994) 1641–1643.
[30] A.A. Tovar, Production and propagation of cylindrically polarized Laguerre–Gaussian Laser beams, Journal of the Optical Society of America 15 (10) (1998) 2705–2711.
[31] F. Gori, M. Santarsiero, R. Borghi, G. Piquero, Use of the van Cittert–Zernike theorem for partially polarized sources, Optical Letters 25 (17) (2000) 1291–1293.
[32] G.P. Agrawal, E. Wolf, Propagation-induced polarization changes in partially coherent optical beams, Journal of the Optical Society of America A 17 (11) (2000) 2019–2023.
[33] F. Gori, M. Santarsiero, G. Piquero, R. Borghi, A. Mondello, R. Simon, Partially polarized Gaussian Schell-model beams, Journal of Optics A 3 (1) (2001) 1–9.
[34] G. Piquero, R. Borghi, M. Santarsiero, Gaussian Schell-model beams propagating through polarization gratings, Journal of the Optical Society of America A 18 (6) (2001) 1399–1405.
[35] G. Piquero, R. Borghi, A. Mondello, M. Santarsiero, Far field of beams generated by quasi-homogeneous sources passing through polarization gratings, Optics Communications 195 (5–6) (2001) 339–350.
[36] Y. Fainman, J. Shamir, Polarization of nonplanar wave fronts, Applied Optics 23 (18) (1984) 3188–3195.
[37] R. Simon, E.C.G. Sudarshan, N. Mukunda, Gaussian–Maxwell beams, Journal of the Optical Society of America A 3 (4) (1986) 536–540.
[38] R. Simon, E.C.G. Sudarshan, N. Mukunda, Cross polarization in laser beams, Applied Optics 26 (9) (1987) 1589–1593.
[39] K.E. Oughstun, Polarization properties of the freely propagating electromagnetic field of arbitrary spatial and temporal form, Journal of the Optical Society of America A 9 (4) (1992) 578–584.

[40] J.F. Nye, J.V. Hajnat, The wave structure of monochromatic electromagnetic radiation, Proceedings of the Royal Society of London 409 (1987) 21–36.
[41] D.G. Hall, Vector-beam solutions of Maxwell's waves equation, Optical Letters 21 (1) (1996) 9–11.
[42] P. Varga, P. Török, Exact and approximate solutions of Maxwell's equation and the validity of the scalar wave approximation, Optical Letters 21 (1) (1996) 1523–1525.
[43] S.R. Seshadri, Electromagnetic Gaussian beam, Journal of the Optical Society of America A 15 (10) (1998) 2712–2719.
[44] P. Varga, P. Török, The Gaussian wave solution of Maxwell's equations and the validity of the scalar wave approximation, Optics Communications 152 (1–3) (1998) 108–118.
[45] S.R. Seshadri, Partially coherent Gaussian Schell-model electromagnetic beam, Journal of the Optical Society of America A 16 (6) (1999) 1373–1380.
[46] C.J.R. Sheppard, S. Saghafi, Electromagnetic Gaussian beams beyond the paraxial approximation, Journal of the Optical Society of America A 16 (6) (1999) 1381–1386.
[47] M.V. Berry, M.R. Dennis, Polarization singularities in isotropic random vector waves, Proceedings of the Royal Society of London 457 (2000) 141–155.
[48] S.R. Seshadri, Average characteristics of partially coherent electromagnetic beams, Journal of the Optical Society of America A 17 (4) (2000) 780–789.
[49] C.J.R. Sheppard, Polarization of almost-planes waves, Journal of the Optical Society of America A 17 (2) (2000) 335–341.
[50] R. Martínez-Herrero, P.M. Mejías, S. Bosch, A. Carnicer, Vectorial structure of nonparaxial electromagnetic beams, Journal of the Optical Society of America A 18 (7) (2001) 1678–1680.
[51] E. Wolf, Coherence properties of partially polarized electromagnetic radiation, Il Nuovo Cimento 13 (6) (1959) 1165–1181.
[52] F. Gori, Matrix treatment for partially polarized, partially coherent beams, Optical Letters 23 (4) (1998) 241–243.
[53] F. Gori, M. Santarsiero, S. Vicalvi, R. Borghi, G. Guattari, Beam coherence-polarization matrix, Journal of the European Optical Society A 7 (5) (1998) 941–951.
[54] E.L. O'Neill, Introduction to Statistical Optics, Addison-Wesley Publ. Co, Reading, MA, 1963.
[55] C. Whitney, Pauli-algebraic operators in polarization optics, Journal of the Optical Society of America 61 (9) (1971) 1207–1213.
[56] R. Martínez-Herrero, J.M. Movilla, P.M. Mejías, Beam propagation through uniaxial anisotropic media: global changes in the spatial profile, Journal of the Optical Society of America A 18 (8) (2001) 2009–2014.
[57] A.E. Siegman, Lasers, Oxford University Press, Oxford, 1986.
[58] J.W. Goodman, Introduction to Fourier Optics, McGraw-Hill, New York, 1968.
[59] J. Perina, Coherence of Light, Van Nostrand Reinhold Company, London, 1971.
[60] M.J. Beran, G.B. Parrent, Theory of Partial Coherence, Prentice-Hall, Englewood Cliffs, NJ, 1967.
[61] M. Born, E. Wolf, Principles of Optics, 7th Edition, Cambridge University Press, Cambridge, 1999.
[62] J.M. Jauch, F. Rohrlich, The Theory of Photons and Electrons, Addison-Wesley Publ. Co, Cambridge, MA, 1955.
[63] R. Barakat, The statistical properties of partially polarized light, Optica Acta 32 (3) (1985) 295–312.
[64] C. Brosseau, R. Barakat, E. Rockower, Statistics of the Stokes parameters for Gaussian distributed fields, Optics Communications 82 (3–4) (1991) 204–208.
[65] C. Brosseau, Statistics of the normalized Stokes parameters for a Gaussian stochastic plane wave field, Applied Optics 34 (22) (1995) 4788–4793.
[66] C. Brosseau, D. Bicout, Entropy production in multiple scattering of light by a spatially random medium, Physical Review E 50 (6) (1994) 4997–5005.
[67] F. Le Roy-Brehonnet, B. Le Jeune, Utilization of Mueller matrix formalism to obtain targets depolarization and depolarization properties, Progress in Quantum Electronics 21 (2) (1997) 109–151.
[68] R. Simon, The connection between the Jones and Mueller matrices, Optics Communications 42 (5) (1982) 293–297.
[69] J.J. Gil, Characteristic properties of Mueller matrices, Journal of the Optical Society of America A 17 (2) (2000) 328–334.

[70] ISO/DIS 12005, Optics and optical instruments—lasers and laser related equipment—test methods for laser beam parameters: polarization (International Organization for Standardization, Geneva, Switzerland).
[71] A. Walther, Radiometry and coherence, Journal of the Optical Society of America 58 (9) (1968) 1256–1259.
[72] A. Walther, Reply to Marchand and Wolf, Journal of the Optical Society of America 64 (9) (1974) 1275.
[73] E.W. Marchand, E. Wolf, Walther's definitions of generalized radiance, Journal of the Optical Society of America 64 (9) (1974) 1273–1274.
[74] R. Martínez-Herrero, P.M. Mejías, On the spatial parametric characterization of general light beams, in: J. Dainty (Ed.), Current Trends in Optics, Vol. II, Academic Press, New York, 1994.
[75] P.M. Mejías, H. Weber, R. Martínez-Herrero, A. González-Ureña (Eds.), Proceedings of the First Workshop on Laser Beam Characterization, SEDO, Madrid, 1993.
[76] H. Weber, N. Reng, J. Lüdtke, P.M. Mejías (Eds.), Proceedings of the Second Workshop on Laser Beam Characterization II, FLI, Berlín, 1994.
[77] M. Morin, A. Giesen (Eds.), Third International Workshop on Laser Beam and Optics Characterization, Proceedings SPIE 2870, The International Society for Optical Engineering, Bellingham, 1996.
[78] A. Giesen, M. Morin (Eds.), Fourth International Workshop on Laser Beam and Optics Characterization, VDI-TechnologieZentrum, Munich, 1998.
[79] H. Laabs, H. Weber (Eds.), Proceedings of the Fifth International Workshop on Laser Beam and Optics Characterization, VDI-TechnologieZentrum, Erice, 2000.
[80] Proceedings of the Sixth International Workshop on Laser Beam and Optics Characterization, Munich, 2001, in press.
[81] J. Serna, P.M. Mejías, R. Martínez-Herrero, Rotation of partially coherent beams propagating through free space, Optical Quantum Electronics 24 (9) (1992) S873–S880.
[82] J. Serna, J.M. Movilla, Orbital angular momentum of partially coherent beams, Optical Letters 26 (7) (2001) 405–407.
[83] G. Piquero, P.M. Mejías, R. Martínez-Herrero, Sharpness changes of Gaussian beams induced by spherically aberrated lenses, Optics Communications 107 (3–4) (1994) 179–183.
[84] R. Martínez-Herrero, G. Piquero, P.M. Mejías, On the propagation of the kurtosis parameter of general beams, Optics Communications 115 (3) (1995) 225–232.
[85] M. Scholl, G. Herziger, Kurtosis as a tool parameter for laser welding, Proceedings of the SPIE 2375 (1995) 130–141.
[86] S.A. Amarande, Beam propagation factor and the kurtosis parameter of flattened Gaussian beams, Optics Communications 129 (5–6) (1996) 311–317.
[87] P. Loosen, K. Du, C. Maier, O. Märten, M. Scholl, Laser beam characterization and measurement techniques, in: P.M. Mejías, H. Weber, R. Martínez-Herrero, A. González-Ureña (Eds.), Proceedings of Laser Beam Characterization, SEDO, Madrid, 1993.
[88] J. Serna, R. Martínez-Herrero, P.M. Mejías, Parametric characterization of general partially coherent beams propagating through ABCD optical systems, Journal of the Optical Society of America A 8 (7) (1991) 1094–1098.
[89] R. Martínez-Herrero, P.M. Mejías, M. Sánchez, J.L.H. Neira, Third- and fourth-order parametric characterization of partially coherent beams propagating through ABCD optical systems, Optical Quantum Electronics 24 (9) (1992) 1021–1026.
[90] R. Martínez-Herrero, P.M. Mejías, C. Martínez, Parametric characterization of the phase at the far field, Optical Letters 20 (7) (1995) 651–653.
[91] R. Martínez-Herrero, P.M. Mejías, On the fourth-order spatial characterization of laser beams: new invariant, Optics Communications 140 (1–3) (1997) 57–60.
[92] S. Lavi, R. Prochaska, E. Keren, Generalized beam parameters and transformation law for partially coherent light, Applied Optics 27 (17) (1988) 3696–3703.
[93] R. Simon, N. Mukunda, E.C.G. Sudarshan, Partially coherent beams and a generalized ABCD-law, Optics Communications 65 (5) (1988) 322–328.

[94] A.E. Siegman, New developments in laser resonators, in D.A. Holmes (Ed.), Optical Resonators, Proceedings SPIE 1224, The International Society for Optical Engineering, Bellingham, 1990, pp. 2–14.
[95] H. Weber, Propagation of higher-order intensity moments in quadratic-index media, Optical Quantum Electronics 24 (9) (1992) 1027–1049.
[96] C. Martínez, Spatial and time characterization of continuous and pulsed light beams, Ph.D. Dissertation, Universidad Complutense, 1998.
[97] G. Nemes, A.E. Siegman, Measurement of all ten second-order moments of an astigmatic beam by the use of rotating simple astigmatic (anamorphic) optics, Journal of the Optical Society of America A 11 (8) (1994) 2257–2264.
[98] J. Serna, F. Encinas-Sanz, G. Nemes, Complete spatial characterization of a pulsed doughnut-type beam by use of spherical optics and a cylindrical lens, Journal of the Optical Society of America A 18 (7) (2001) 1726–1733.
[99] R. Martínez-Herrero, P.M. Mejías, J.M. Movilla, Spatial characterization of partially polarized beams, Optical Letters 22 (4) (1997) 206–208.
[100] S.A. Collins Jr., Lens-system Diffraction Integral written in terms of matrix optics, Journal of the Optical Society of America 60 (9) (1970) 1168–1177.
[101] J.M. Movilla, Spatial parametrization of light beams: some aspects concerning polarization. Ph.D. Dissertation, Universidad Complutense, 2000.
[102] J.M. Movilla, G. Piquero, R. Martínez-Herrero, P.M. Mejías, Parametric characterization of non-uniformly polarized beams, Optics Communications 149 (4–6) (1998) 230–234.
[103] J.M. Movilla, G. Piquero, R. Martínez-Herrero, P.M. Mejías, On the measurement of the generalized degree of polarization, Optical Quantum Electronics 32 (12) (2000) 1333–1342.
[104] Q. Lü, S. Dong, H. Weber, Analysis of TEM_{00} laser beam quality degradation caused by a birefringent Nd:YAG rod, Optical Quantum Electronics 27 (9) (1995) 777–783.
[105] N. Kugler, S. Dong, Q. Lü, H. Weber, Investigation of the misalignment sensitivity of a birefringence compensated two-rod Nd:YAG laser system, Applied Optics 36 (36) (1997) 9359–9366.
[106] G. Piquero, J.M. Movilla, P.M. Mejías, R. Martínez-Herrero, Degree of polarization of non-uniformly partially polarized beams: a proposal, Optical Quantum Electronics 31 (3) (1999) 223–225.
[107] A.T. Friberg (Ed.), Selected Papers on Coherence and Radiometry, SPIE Milestone Series, MS 69, The International Society for Optical Engineering, Bellingham, 1993.
[108] F. Gori, Mode propagation of the field generated by Collett–Wolf sources, Optics Communications 46 (3–4) (1983) 149–154.
[109] G. Piquero, F. Gori, P. Romanini, M. Santarsiero, R. Borghi, A. Mondello, Synthesis and characterization of partially polarized Gaussian Schell-model sources, Proceedings of the Sixth International Workshop on Laser Beam and Optics Characterization, Munich, June 2001, in press.
[110] ISO/DIS 11146, Optics and optical instruments—lasers and laser related equipment- test methods for laser beam parameters: beam widths, divergence angle and beam propagation factor (International Organization for Standardization, Geneva, Switzerland) 1999.
[111] R. Martínez-Herrero, P.M. Mejías, G. Piquero, Quality improvement of partially coherent symmetric-intensity beams caused by quartic phase distorsions, Optical Letters 17 (23) (1992) 1650–1651.
[112] J. Serna, P.M. Mejías, R. Martínez-Herrero, Beam quality changes of Gaussian Schell-model fields propagating through Gaussian apertures, Applied Optics 31 (22) (1992) 4330–4331.
[113] R. Martínez-Herrero, P. M. Mejías, Quality improvement of symmetric-intensity beams propagating through pure phase plates, Optics Communications 95 (1–3) (1993) 18–20.
[114] A.E. Siegman, Analysis of laser beam quality degradation caused by spherical aberration, Applied Optics 32 (30) (1993) 5893–5901.
[115] A.E. Siegman, Binary phase plates cannot improve laser beam quality, Optical Letters 18 (9) (1993) 675–677.
[116] J.A. Ruff, A.E. Siegman, Measurement of beam quality degradation due to spherical aberration in a simple lens, Optical Quantum Electronics 26 (6) (1994) 629–632.

[117] L.W. Casperson, Phase plates transform laser beam, Laser Focus World 30 (5) (1994) 223–228.
[118] J.M. Movilla, R. Martínez-Herrero, P.M. Mejías, Quality improvement of partially polarized beams, Applied Optics 40 (33) (2001) 6098–6101.
[119] G. Piquero, J.M. Movilla, R. Martínez-Herrero, P.M. Mejías, Beam quality of partially polarized beams propagating through lens-like birefringent elements, Journal of the Optical Society of America A 16 (11) (1999) 2666–2668.